Available online at www.sciencedirect.com
SCIENCE DIRECT®
Continental Shelf Research 25 (2005) 2233–2260
CONTINENTAL SHELF RESEARCH
www.elsevier.com/locate/csr

A 3D boundary-fitted barotropic hydrodynamic model for the New York Harbor region

S. Sankaranarayanan*

Applied Science Associates, 70, Dean Knauss Drive, Narragansett, RI-02882, USA

Received 7 April 2004; received in revised form 25 April 2005; accepted 10 August 2005
Available online 28 October 2005

Abstract

A three-dimensional barotropic hydrodynamic model application to the New York Harbor Region is performed using the Boundary-Fitted HYDROdynamic model (BFHYDRO). The model forcing functions consist of surface elevations along the open boundaries, hourly winds, and fresh water flows from the rivers and sewage flows. A comprehensive skill assessment of the model predictions is done using observed surface elevations and three-dimensional currents. The model-predicted surface elevations compare well with the observed surface elevations at four stations. Mean errors in the model-predicted surface elevations are less than 4% and correlation coefficients exceed 0.985. Model-predicted three-dimensional currents at Verrazano Narrows show excellent comparison with the observations, with mean errors less than 11% and correlation coefficients exceeding 0.960. Model-predicted three-dimensional currents at Bergen Point compare well with the observations, with mean errors less than 15% and correlation coefficients exceeding 0.897. The surface elevation amplitudes and phases of the principal tidal constituents at nine tidal stations, obtained from a harmonic analysis of a 60-day simulation compare well with the observed data. The predicted amplitude and phase of the M_2 tidal constituent at these stations are, respectively, within 5 cm and 6° of the observed data. The model-predicted tidal ellipse parameters for the major tidal constituents compare well with the observations at Verrazano Narrows and Bergen Point. The model-predicted along channel sub-tidal currents also compare well with the observations. The semi-diurnal tidal ranges and spring and neap tidal cycles of the surface elevations and currents are well reproduced in the model at all stations. The observed currents at Bergen Point were shown to be flood dominant through tidal distortion analysis. The model-predicted currents also showed Newark Bay and Arthur Kill to be flood dominant systems. The model predictions showed the occurrence of a pronounced flow separation and formation of a pair of counter-rotating eddies in the Lower New York Bay. The model-predicted residual circulation pattern showed many gyres in the Harbor Region and Jamaica Bay.

Keywords: New York Harbor; Barotropic; Boundary-fitted; Hydrodynamic modeling

1. Introduction

Tides in the New York Harbor are predominantly semi-diurnal, with M_2 being the dominant constituent. The amplitude of the M_2 harmonic constituent at Willets Point (Fig. 1) is about 60% higher than at Sandy Hook (Fig. 1). High water at Willet Point occurs about $3\frac{3}{4}$h later than the high water at Sandy Hook. This difference in water surface elevation drives strong tidal currents in the New York Harbor,

*Tel.: +1 401 7896224; fax: +1 401 7891932.
E-mail address: sankar@appsci.com.

0278-4343/$ - see front matter © 2005 Elsevier Ltd. All rights reserved.
doi:10.1016/j.csr.2005.08.022

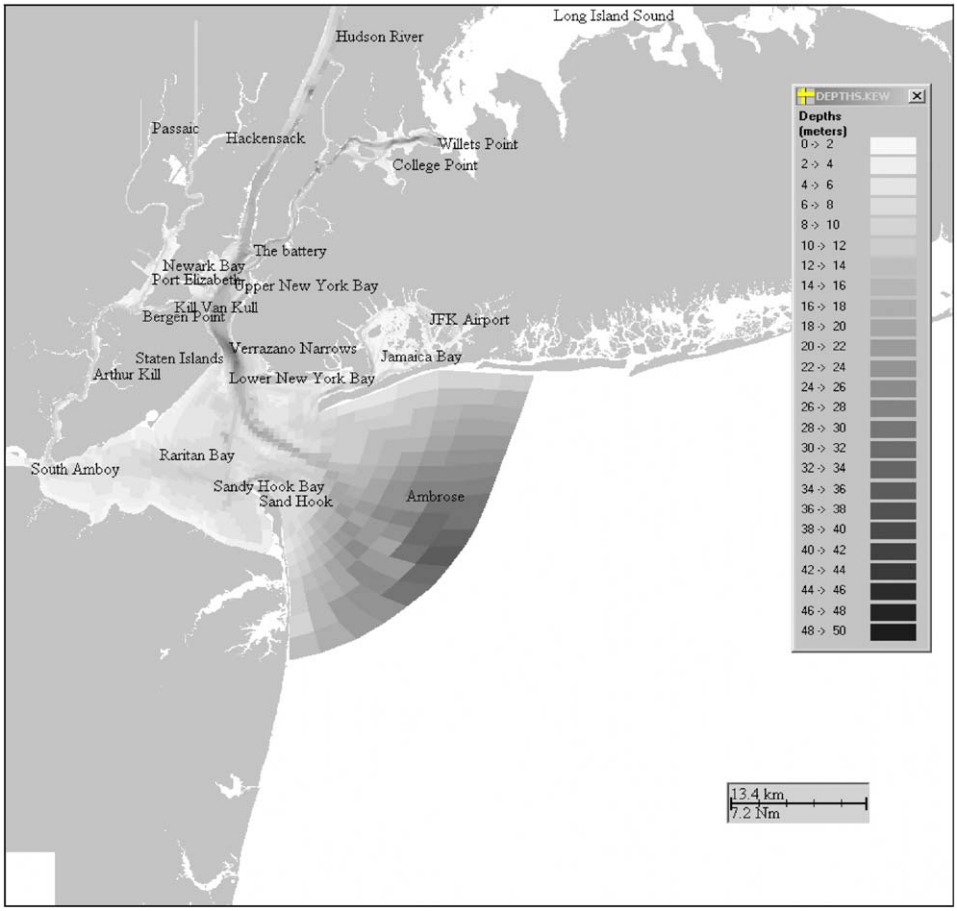

Fig. 1. The study area and its bathymetry.

with currents exceeding 1.2 m/s at Verrazano Narrows.

Three-dimensional Hydrodynamic modeling studies of the New York Harbor region have been done in the past to understand the estuarine circulation produced by tidal forcing and fresh water flows. Oey et al. (1985) have reported a numerical model of the Hudson-Raritan Estuary, comparing the model results with short-term data. Due to the very coarse resolution of their model grid, Jamaica Bay was not included in their model domain. They approximated Jamaica Bay as a constant depth bay of approximately equal volume. Scheffener et al. (1994) developed a coupled three-dimensional model of New York Bight, Long Island Sound, and New York Bay. Model calibration and validation performed for short periods showed a lot of discrepancies between model and data, for currents, salinity and temperature. Blumberg and Pritchard (1997) investigated the hydrodynamic characteristics of the East River using the Estuarine Coastal Ocean Model (ECOM) developed by Blumberg and Mellor (1987). The model was calibrated and validated through comparisons with measured salinities, water levels, current velocities and data-based estimates of volume flux. Blumberg et al. (1999) studied the estuarine circulation in the New York Harbor complex, Long Island Sound and the New York Bight using ECOM, within the framework of a single grid system. The predicted tidal elevations, currents, salinities and temperatures compared well with the observations.

In the present study, a three-dimensional hydrodynamic modeling of New York Harbor region is performed, using a three-dimensional boundary-fitted hydrodynamic model to obtain the circulation pattern in the area. The modeling domain encompasses Hudson River up to Dobbs Ferry, parts of

Long Island Sound up to Willets Point, East River, Raritan Bay, Newark Bay, Sandy Hook Bay and Jamaica Bay. The main limitation of the present study is that the effects of stratification and estuarine flow are not considered and hence the interactions between the estuarine flow and tides are ignored. The primary objective of this modeling study is to provide a better resolution of the harbor region and reproduce the observed vertical variations in the currents. A comprehensive skill assessment of the model predictions is done using observed surface elevations and three-dimensional currents. The degree of non-linear tidal distortion in the observed and model-predicted currents is studied. The model-predicted tide-induced residual currents in the Harbor Region are also presented.

2. Sources of available data in New York Harbor region

Time series of currents and surface elevations recorded by National Oceanic and Atmospheric Administration (NOAA) at selected stations, available at http://co-ops.nos.noaa.gov/nyports/nyports.html, are used as the primary data to validate the model. The harmonic tidal constituents of surface elevations and currents published by NOAA are used to calibrate the model. Hourly fresh water flows for the Hudson River obtained from United States Geological Survey (USGS) is also used. The mean river flows from other fresh water sources given in Oey et al. (1985a) are used as the fresh water flows into the New York Harbor region. Hourly winds obtained from the Bergen Point

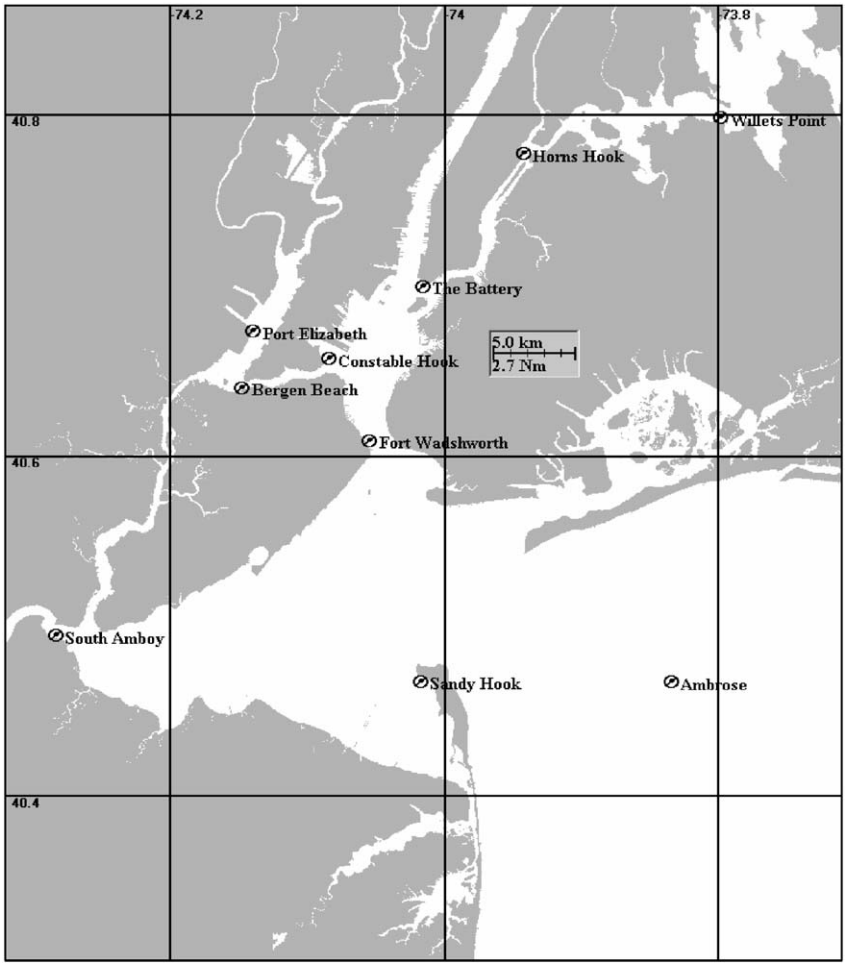

Fig. 2. Locations of tidal stations.

meteorological station are used as the wind forcing over the study area.

3. Model description

The hydrodynamic model used in the present study is the three-dimensional time-dependent generalized non-orthogonal boundary-fitted model in spherical coordinates developed by Muin and Spaulding (1997a). This model, called BFHYDRO, has been successfully applied to coastal and estuarine waters. Some recent applications of the model include the Mount Hope Bay (Swanson et al., 2005), Providence River (Muin and Spaulding, 1997b), Bay of Fundy (Sankaranarayanan and French McCay, 2003a) and San Francisco Bay (Sankaranarayanan and French McCay, 2003b). The model solves a coupled system of partial differential prognostic equations describing conservation of mass, momentum, salt and temperature in a generalized non-orthogonal boundary-fitted coordinate system. The equations of continuity and motion on a spherical coordinate system are given below.

Continuity Equation:

$$\frac{1}{r\cos\theta}\frac{\partial u}{\partial\phi}+\frac{1}{r}\frac{\partial v}{\partial\theta}-\frac{v}{r}\tan\theta+\frac{1}{r^2}\frac{\partial r^2 w}{\partial r}=0. \tag{1}$$

Momentum equation in ϕ-direction:

$$\frac{\partial u}{\partial t}+\frac{u}{r\cos\theta}\frac{\partial u}{\partial\phi}+\frac{v}{r}\frac{\partial u}{\partial\theta}-\frac{uv}{r}\tan\theta+w\frac{\partial u}{\partial r}+\frac{uw}{r}-fv=-\frac{1}{\rho_0 r\cos\theta}\frac{\partial p}{\partial\phi}+\frac{\partial}{\partial r}\left(A_v\frac{\partial u}{\partial r}\right). \tag{2}$$

Momentum equation in θ-direction:

$$\frac{\partial v}{\partial t}+\frac{u}{r\cos\theta}\frac{\partial v}{\partial\phi}+\frac{v}{r}\frac{\partial v}{\partial\theta}-\frac{uu}{r}\tan\theta+w\frac{\partial v}{\partial r}+\frac{vw}{r}+fu=-\frac{1}{\rho_0 r}\frac{\partial p}{\partial\theta}+\frac{\partial}{\partial r}\left(A_v\frac{\partial v}{\partial r}\right). \tag{3}$$

Fig. 3. Locations of tidal current stations.

Momentum equation in r-direction:

$$\frac{\partial p}{\partial r} = -\rho_0 g, \tag{4}$$

where ϕ is the longitude positive east, θ is the latitude positive north, r is positive up, u, v and w are the velocities in ϕ, θ and r directions respectively; f is the Coriolis parameter, g is gravity, ρ_0 is the reference density, and A_v is the vertical eddy viscosity. Eqs. (1)–(4) assume the following: the flow incompressible, density differences are neglected unless multiplied by gravity (Boussinesq approximation), the vertical acceleration is small compared to gravity (hydrostatic assumption) and the horizontal stresses are neglected.

Eqs. (1)–(4) are transformed to a σ-coordinate system in the vertical plane and a generalized non-orthogonal coordinate system in the horizontal plane. The fully transformed equations are given in Muin and Spaulding (1997a).

Boundary conditions:

At the surface $\sigma = 0$,

$$\frac{A_v}{D}\left(\frac{\partial u}{\partial \sigma}, \frac{\partial v}{\partial \sigma}\right) = \gamma_s\left(\sqrt{W_\phi^2 + W_\theta^2}\right)(W_\phi, W_\theta). \tag{5}$$

At the bottom $\sigma = -1$,

$$\frac{A_v}{D}\left(\frac{\partial u}{\partial \sigma}, \frac{\partial v}{\partial \sigma}\right) = C_d\left(\sqrt{{u_b}^2 + {v_b}^2}\right)(u_b, v_b), \tag{6}$$

where c_d is the quadratic bottom drag coefficient, γ_s is the surface wind stress coefficient, u_b and v_b are the velocities at the bottom sigma level, and W_ϕ and W_θ are the wind speeds, respectively, in ϕ and θ directions.

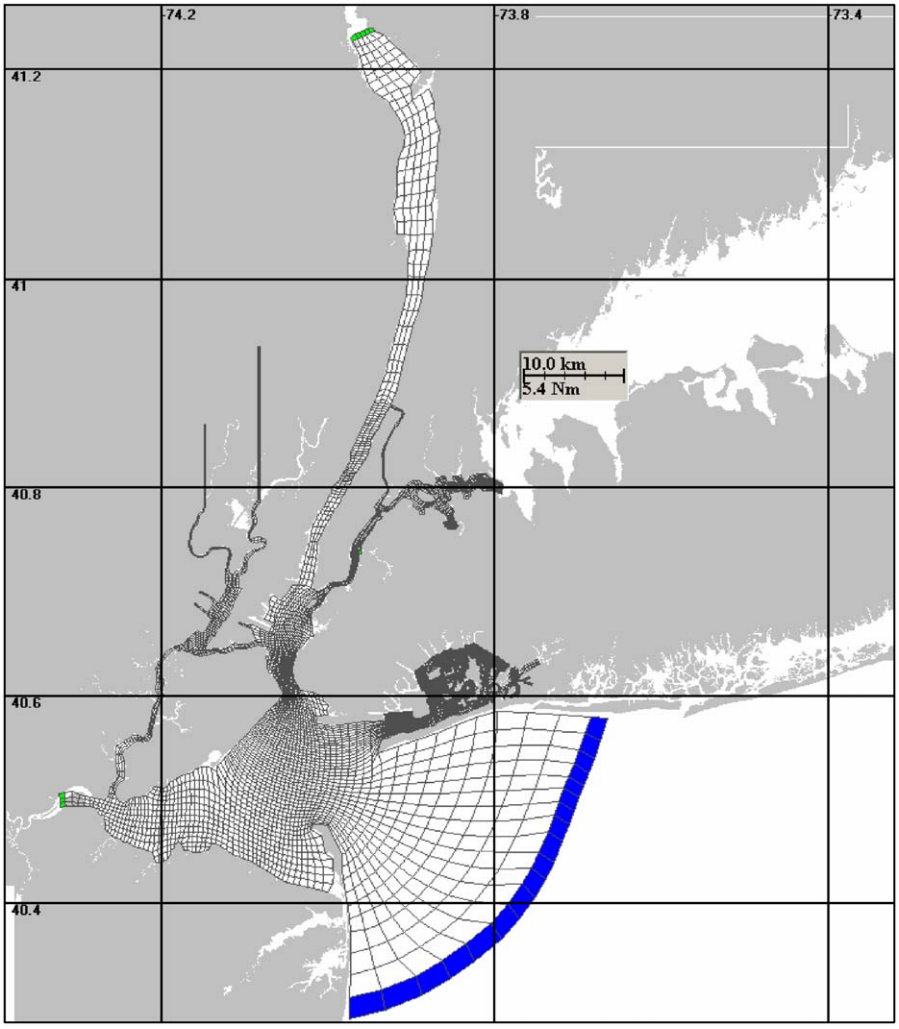

Fig. 4. Boundary-fitted grid of the study area.

The vertical boundary conditions are

$$\omega = 0 \text{ at } \sigma = 0 \text{ and } s = -1. \quad (7)$$

At the land boundaries, the normal component of the velocity is set to zero. At the open boundaries, the water surface elevation is specified as a function of time. The river boundaries are given by a specified inflow-velocity and horizontal pressure gradient is set to zero.

The equations of motion (Eqs. (1)–(4)) are split into exterior and interior modes to increase the allowable time step and hence reduce the computational time. Solution of the exterior mode using a semi-implicit solution methodology has been described in Muin and Spaulding (1996). The vertical diffusion term for the interior mode is solved implicitly using a three-time level scheme. The spatial discretization is based on a space staggered C-grid system (Arakawa and Lamb, 1977) and the temporal discretization is based on three level scheme with a weighting factor of 1.5. Thus, the algorithm is second order in time and space. The boundary-fitted model technique matches the model coordinates with the shoreline boundaries and allows the user to adjust the model grid resolution as desired. Thus, the system allows the user to use a very fine grid resolution in Jamaica Bay and New York Harbor with the grid closely fitting the coastline, and a coarse grid resolution in New York Bight.

Fig. 1 shows the study area and its bathymetry. The bathymetry used in the model was taken from digitized NOAA bathymetry and NOAA charts. Figs. 2 and 3 show, respectively, the tidal elevation and tidal current station locations, for model calibration and validation. The boundary-fitted grid for the study area is shown in Fig. 4. The modeling domain encompasses Hudson River up to Dobbs Ferry, parts of Long Island Sound up to Willets Point, East River, Raritan Bay, Newark Bay, Arthur Kill and Jamaica Bay. The transformed grid in the computational plane is shown in Fig. 5. Details of the grid in the Harbor Region are shown in Fig. 6. The ability of boundary-fitted grid system to use variable grid lengths is clearly seen in Fig. 6. The grid consists of 192×179 segments with 11058

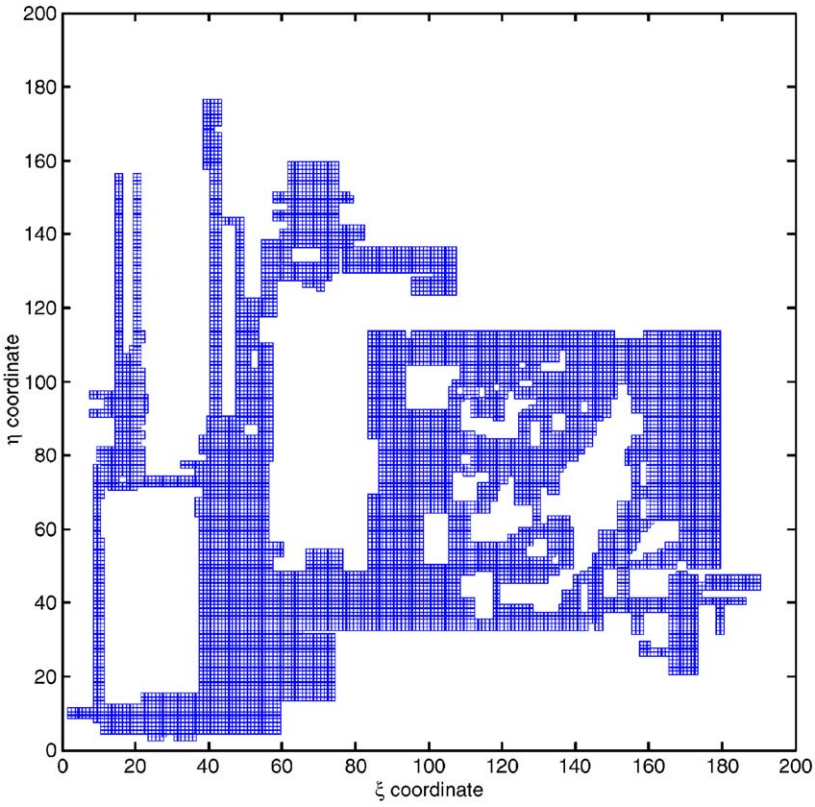

Fig. 5. Boundary-fitted grid in the transformed plane.

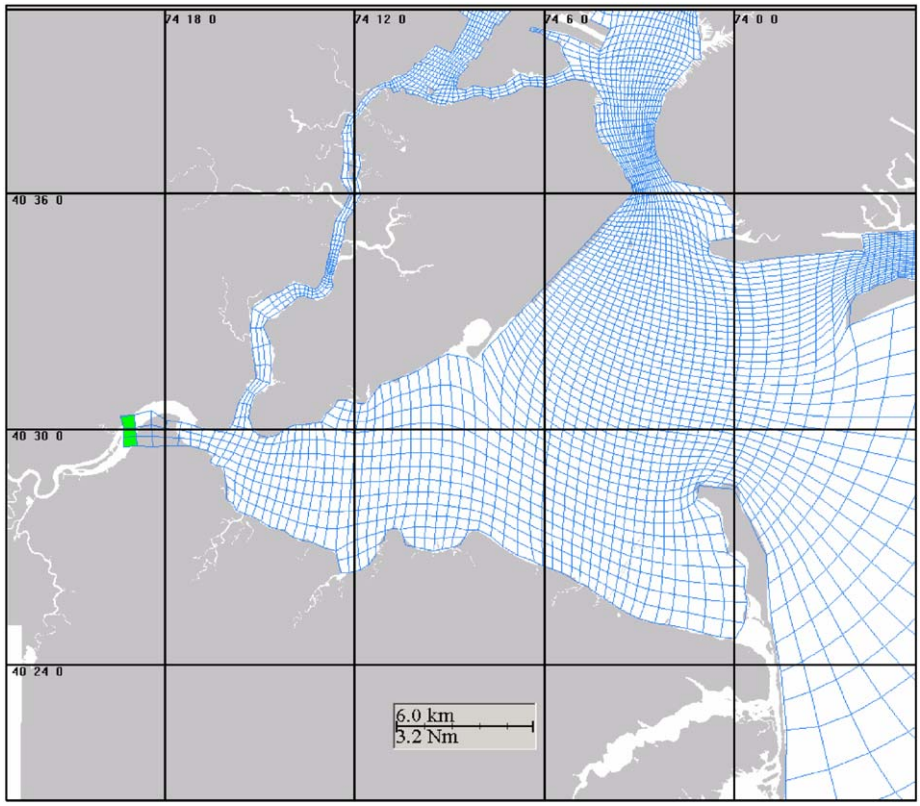

Fig. 6. Detail of the boundary-fitted grid near New York Harbor.

water cells in the horizontal plane and 22 sigma levels in the vertical. The bathymetry was mapped onto the boundary-fitted grid. Table 1 gives a summary of grid cell corners for various grid angle ranges for the boundary-fitted grid shown in Fig. 4. A grid angle of 90° represents an orthogonal grid. It can be seen from Table 1 that 92% of grid cell corners have grid angles greater than 60°. The grid resolution is about 2000 m near the open boundary, about 300 m in the New York Harbor region, about 100 m in the Jamaica Bay. Taking the average depths of water to be 25, 20, and 3 m, respectively in the Outer Bay, Harbor Region and Jamaica Bay, the grid resolution works out to be 350, 2000 and 280 grids per wavelength for the semi-diurnal tide. These grid resolutions were shown to be adequate enough to model the tidal circulation (Sankaranarayanan and Spaulding, 2003). The grid system was designed to provide sufficient resolution in the New York Harbor region and a fine resolution in the Jamaica Bay, to study the residual circulation.

Table 1
Range of grid angles for the grid

Range of grid angle (°)	No. of grid cell corners
0–30	19
30–40	143
40–50	504
50–60	2525
60–70	7350
70–80	10983
80–90	22297

4. Model forcing functions

A comparison of the observed winds at Bergen Point and Sandy Hook (Fig. 7) shows that winds at Bergen Point are stronger than that at Sandy Hook. The wind stress calculated from the winds at Bergen Point is applied over the whole domain. Simulations with the application of the wind stress, based on the

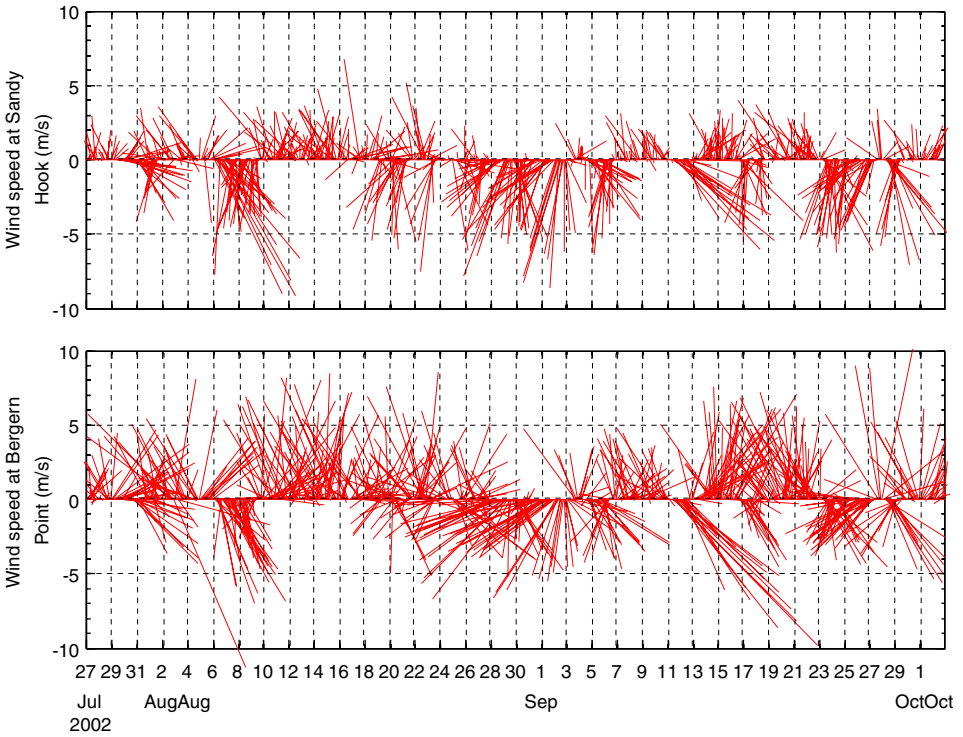

Fig. 7. Comparison of wind speeds at Bergen Point and Sandy Hook.

Table 2
Observed amplitudes and phases of different tidal constituents in Ambrose and Willets Point

Constituent	Ambrose (Moody et al., 1984)		Willets Point (NOAA)	
	Amp (m)	Phase (°)	Amp (m)	Phase (°)
M_2	0.650	208.1	1.103	331.2
N_2	0.156	193.8	0.224	312.1
S_2	0.135	228.0	0.183	352.2
K_1	0.103	100.8	0.099	117.8
O_1	0.063	88.3	0.064	150.9
K_2			0.054	350.8
L_2			0.052	353.2
NU_2			0.050	312.4
P_1			0.029	131.3
$2N_2$			0.027	293.4
M_4			0.036	217.4
M_6			0.077	85.2

winds at Sandy Hook, did not alter the circulation pattern in the study area. The major tidal constituents for the tidal station at Ambrose (Moody et al., 1984) and Willets Point (NOAA) are given in Table 2. The difference in surface elevation harmonics between Ambrose and Willets Point for the M_2 tidal constituent is clearly seen in Table 2 with amplitudes varying by a factor 1.7 and phases differing by 120°. This difference in surface elevation harmonics between Ambrose and Willets Point drives strong tidal currents in the East River and New York Harbor region. A comparison of the observed 32-h low-passed sub-tidal surface elevations at four tidal stations inside the harbor region is shown in Fig. 8. The sub-tidal surface elevations at Bergen Point, The Battery and Horns Hook are nearly identical, while the sub-tidal surface elevation at Sandy Hook differs by about 3–5 cm from the other stations. The tidal elevation obtained from a harmonic composition of tidal constituents at Ambrose Light House is added to the 32-h low-passed sub-tidal elevation at Sandy Hook and used as the surface elevation forcing along the open boundary near Ambrose Light House. Similarly, the tidal elevation obtained from a harmonic composition of tidal constituents at Willets Point is added to the 32-h low-passed sub-tidal elevation at Kings Point and used as the surface elevation forcing along the open boundary at Willets Point. Hourly fresh water flows from the Hudson River into the

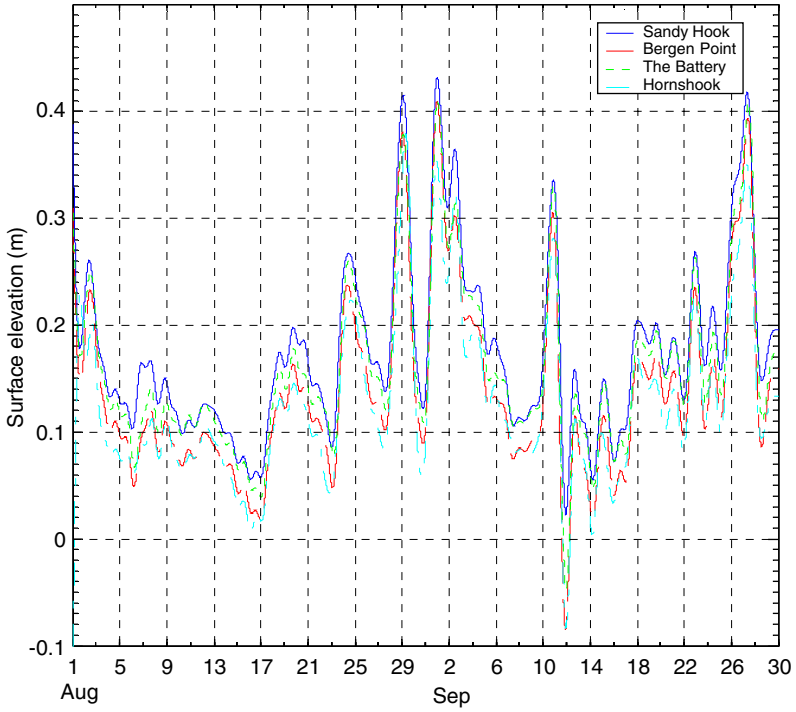

Fig. 8. Comparison of 32-h observed low-passed surface elevation at four stations in New York Harbor.

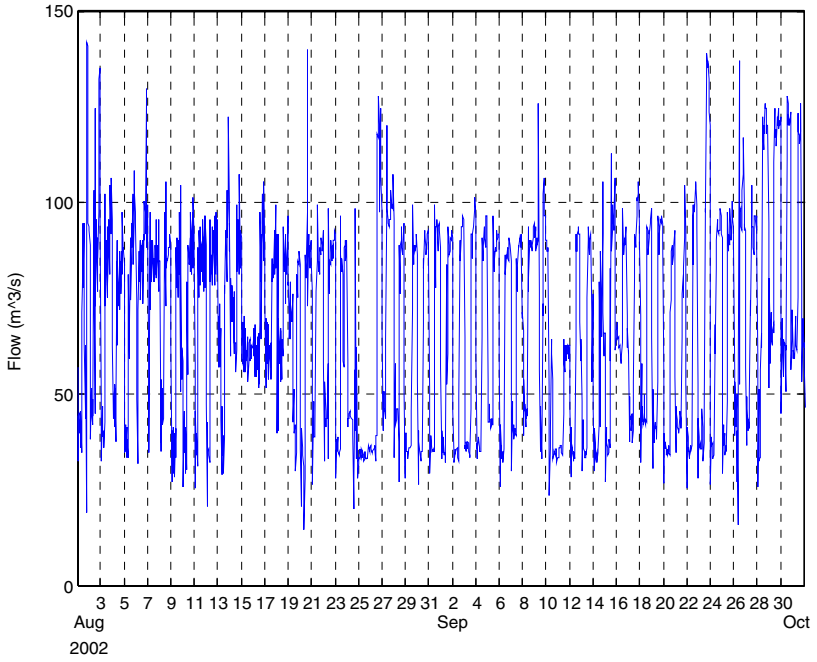

Fig. 9. Hourly fresh water flows from Hudson river into New York Harbor.

New York Harbor as shown in Fig. 9, and mean flows from other fresh water sources (Oey et al., 1985) as given in Table 3 are used as the river flows into the study area.

5. Model skill assessment

Observations of surface elevations at four stations for the period August–September 2002, made

available online by NOAA, was obtained from http://www.coops.nos.noaa.gov. The model calibration was performed, varying the bottom friction coefficient from 0.001 to 0.005. The vertical eddy viscosity (A_v) is varied between 0.001 and 0.1 m^2/s to match the vertical structure of the observed currents. A constant wind stress coefficient of 0.0015 is used.

Table 3
Mean freshwater flows including sewage into NewYork Harbor

River	Mean flows (m^3/s)
Hudson	130
Raritan	8
Passaic	3
East River	40
Hackensack	5
Jamaica Bay	14

5.1. Surface elevations

Comparison of the errors in the model-predicted tidal harmonics of surface elevations with the observed data showed that best results were obtained while using a bottom friction coefficient of 0.005. The predicted amplitudes and phases (Eastern Standard Time) were obtained from a harmonic analysis of the 60-day model-predicted surface elevations. A comparison of the observed and predicted amplitudes and phases at nine stations is given in Table 4. The predicted harmonic amplitudes and phases for the M_2 tidal constituent are, respectively, within 5 cm and 7°. The errors (Tables 5 and 6) in the computed phases for the N_2 and S_2 tidal harmonics are slightly higher. However, their strengths are relatively smaller when compared to M_2.

Figs. 10(a) and (b) compare water level elevations at Sandy Hook, Bergen Point and The Battery for a

Table 4
Comparison of M_2 tidal elevation constituents

Station	Source of observed data	Amplitude (m)		Diff.	Phase (°)		Diff.
		Field	Model		Field	Model	
Willets Point	NOAA	1.103	1.086	0.017	331.20	331.5	−0.30
Horns Hook	NOAA	0.675	0.650	0.025	309.10	310.8	−1.70
The Battery	NOAA	0.671	0.686	−0.015	234.40	238.6	−4.20
Port Elizabeth	NOAA	0.749	0.798	−0.049	239.70	233.6	6.10
Constable Hook	NOAA	0.680	0.704	−0.024	229.70	230.8	−1.10
Bergen Beach	NOAA	0.745	0.770	−0.025	236.20	231.9	4.30
Fort Wadsworth	NOAA	0.661	0.696	−0.035	224.30	225.5	−1.20
South Amboy	NOAA	0.713	0.760	−0.047	227.30	220.3	7.00
Sandy Hook	NOAA	0.693	0.710	−0.017	222.50	216.7	5.80

Table 5
Comparison of N_2 tidal elevation constituents

Station	Source of observed data	Amplitude (m)		Diff.	Phase (°)		Diff.
		Field	Model		Field	Model	
Willets Point	NOAA	0.224	0.214	0.010	312.10	320.4	−8.30
Horns Hook	NOAA	0.161	0.132	0.029	287.90	295.6	−7.70
The Battery	NOAA	0.149	0.163	−0.014	218.70	226.4	−7.70
Port Elizabeth	NOAA	0.161	0.192	−0.031	226.80	225.1	1.70
Constable Hook	NOAA	0.163	0.169	−0.006	219.20	220.1	−0.90
Bergen Beach	NOAA	0.166	0.185	−0.019	222.90	222.7	0.20
Fort Wadsworth	NOAA	0.141	0.168	−0.027	212.10	215.5	−3.40
South Amboy	NOAA	0.141	0.184	−0.043	220.80	212.1	8.70
Sandy Hook	NOAA	0.157	0.172	−0.015	207.50	208.2	−0.70

Table 6
Comparison of S_2 tidal elevation constituents

Station	Source of observed data	Amplitude (m)		Diff.	Phase (°)		Diff.
		Field	Model		Field	Model	
Willets Point	NOAA	0.183	0.192	−0.009	352.20	345.7	6.50
Horns Hook	NOAA	0.120	0.116	0.004	323.70	320.1	3.60
The Battery	NOAA	0.133	0.15	−0.017	255.30	249.7	5.60
Port Elizabeth	NOAA	0.141	0.175	−0.034	266.80	248.1	18.70
Constable Hook	NOAA	0.132	0.155	−0.023	255.70	243.2	12.50
Bergen Beach	NOAA	0.143	0.169	−0.026	261.20	245.7	15.50
Fort Wadsworth	NOAA	0.121	0.153	−0.032	245.90	238.5	7.40
South Amboy	NOAA	0.124	0.167	−0.043	247.40	234.8	12.60
Sandy Hook	NOAA	0.137	0.156	−0.019	245.40	230.9	14.50

60-day period. The model-predicted surface elevations compare well with the observations. Statistical evaluation of the model performance for water level elevations is presented in Table 7. Root Mean Square (RMS) errors are less than 4% of the local tidal range and correlation coefficients exceed 0.985. Figs. 11(a) and (b) show, respectively, a comparison of the observed and predicted 32-h low-passed surface elevation at Bergen and The Battery. A statistical evaluation of the 32-h low-passed surface elevations is given in Table 8. The RMS errors in the model-predicted 32-h low-passed surface elevations are less than 4 cm and the correlation coefficients exceed 0.975.

5.2. Current velocities

The Acoustic Doppler Profiler (ADP) current data at two stations namely, Bergen Point and Verrazano Narrows for the period August–September, 2002, was obtained from NOAA/NOS. A fifth-order Butterworth filter, with the cutoff frequency at 8 cycles/day is used to remove the high-frequency signal from the data. The phase shift inherent in the Butterworth filter is eliminated, by passing the data forward and backward through the filter.

Comparisons of the observed and model-predicted three-dimensional currents at Verrazano Narrows and Bergen Point showed that best matching with minimum errors were obtained using a vertical eddy viscosity of $0.05\,m^2/s$.

Comparisons of the observed and predicted three-dimensional currents for a 25-day period at near-surface, mid-depth, and bottom at Verazano Narrows are shown in Figs. 12(i) and (ii). The model clearly reproduces the vertical structure of the current and the spring and neap tidal cycles. The observed and model-predicted current directions at Narrows did not show any significant variation in the vertical direction. The model-predicted current directions at mid-depth compares well with the observations shown in Fig. 12(iii). A statistical evaluation of the model-predicted three-dimensional currents is given in Table 9. A maximum RMS error of 11% and the lowest correlation coefficient of 0.961 are found to occur near the bottom (Table 10).

Tidal current harmonics for the observed and model-predicted currents for a 60-day period were performed using Harmonic analysis (Foreman, 1978). A comparison of the observed and model-predicted M_2 harmonic principal current speeds and directions (Table 13) at Verrazano Narrows shows that the observed tidal currents are well reproduced by the model at all depths. The errors in the model-predicted M_2 principal current speeds are less than 13% of the observations. The model-predicted principal current directions and phases are within 10° of the observations. The minor axis currents are very small. The model-predicted tidal ellipse parameters for the N_2, S_2, K_1, O_1, and L_2 harmonic constituents at mid-depth also show very good comparison with the observations (Tables 11(a) and (b)).

Comparisons of the observed and predicted 32-h low-passed current components at the bottom, mid-depth, and surface are shown, respectively, in Figs. 13(a)–(c). It is to be noted that the observed currents were detrended to remove the mean current from the data in Figs. 13(a)–(c), since baroclinic effects are not included in the model. The model reproduces the sub-tidal variability in the north–south

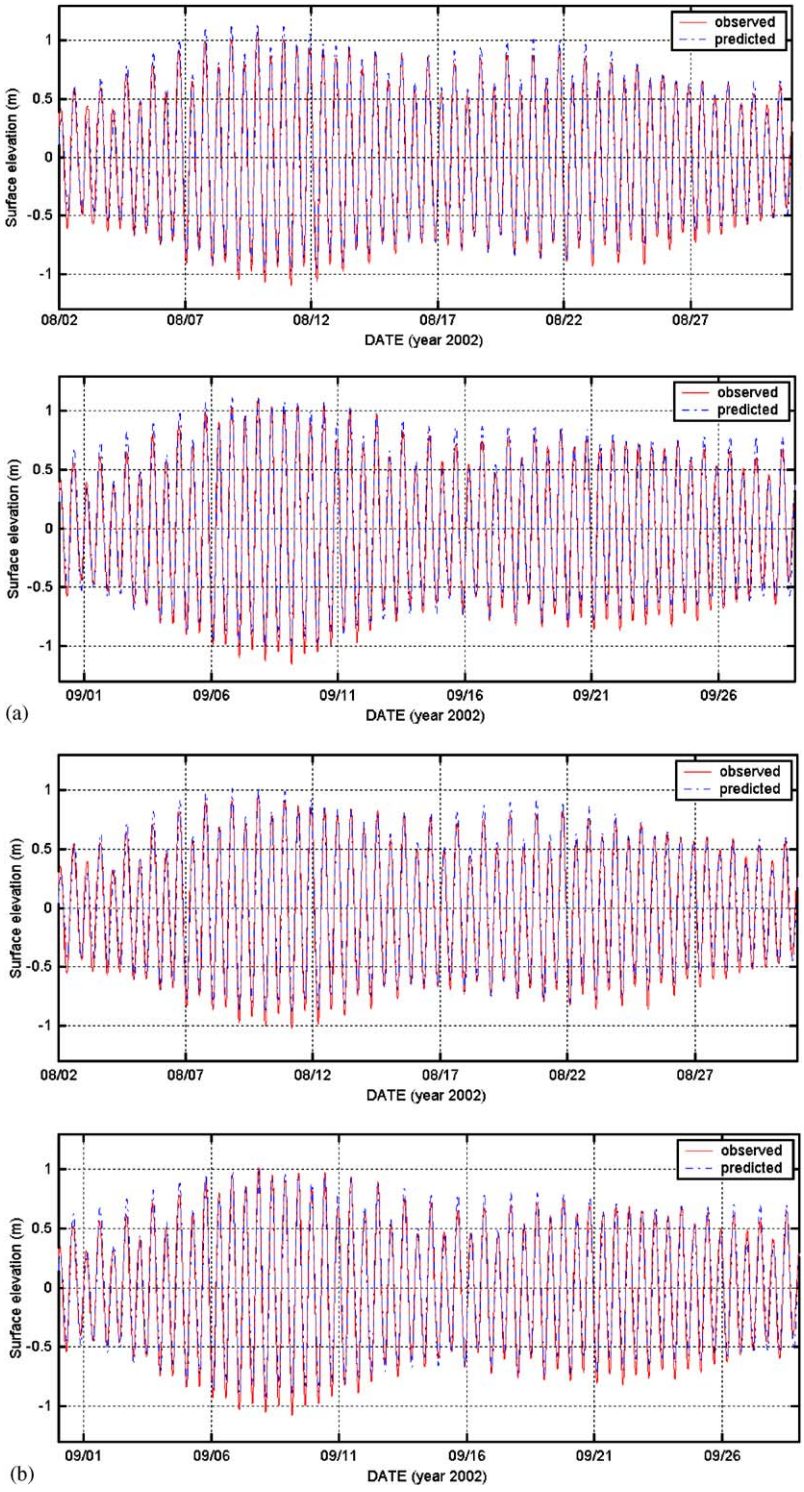

Fig. 10. (a) Comparison of observed and predicted surface elevations at Bergen Point, (b) comparison of observed and predicted surface elevations at The Battery.

Table 7
Statistical evaluation of model performance for instantaneous elevation

Station	Number of data points	Data range (m)	RMS error	RMS error (%)	Correlation coefficient
Sandy Hook	14401	2.180	0.070	3.19	0.991
Bergen Point	14401	2.273	0.077	3.37	0.990
The Battery	14401	2.037	0.088	4.18	0.985
Horns Hook	14401	2.061	0.085	4.11	0.987

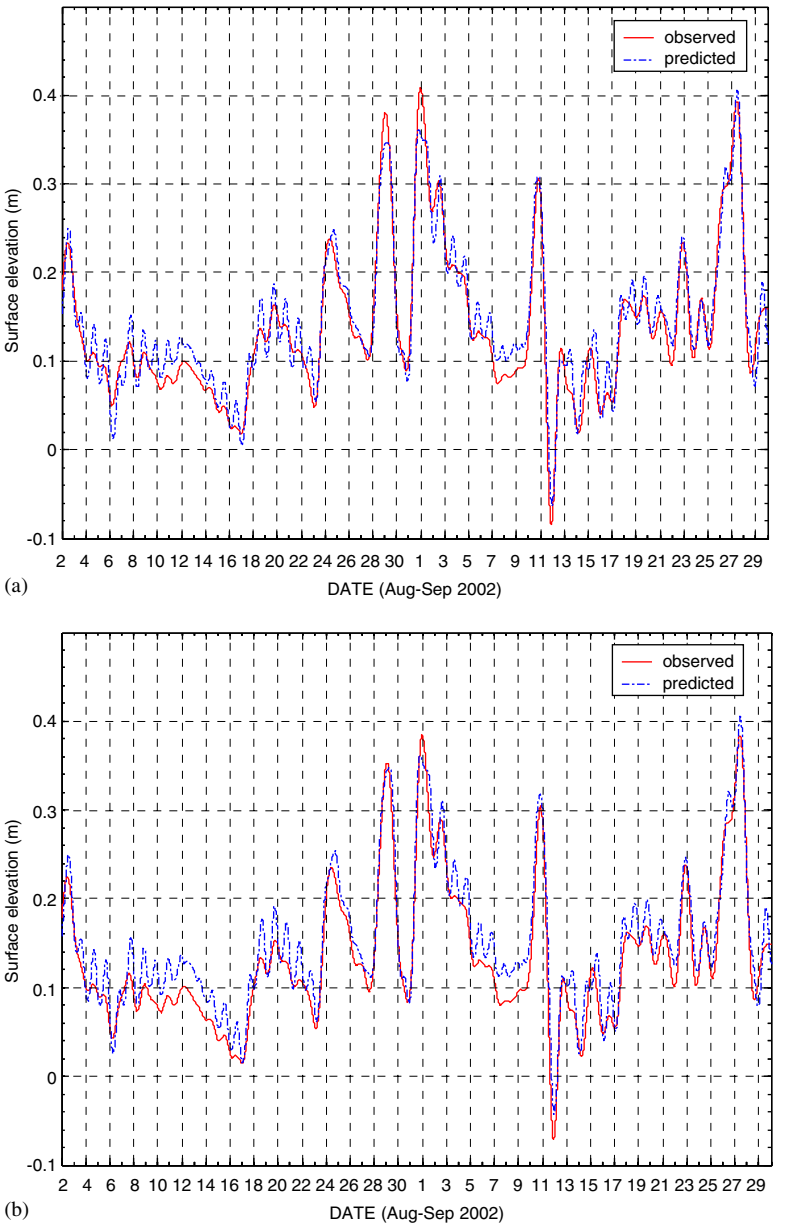

Fig. 11. (a) Comparison of observed and predicted 32-h low-passed water level at Bergen Point, (b) comparison of observed and predicted 32-h low-passed water level at The Battery.

Table 8
Statistical evaluation of model performance for 32-h low-passed water elevations

Station	RMS error (cm)	RMS error (%)	Correlation coefficient
Hornshook	2.8	13.6	0.980
The Battery	2.2	13.7	0.977
Bergen Point	1.9	11.9	0.975

direction, very well in terms of amplitudes and phases. However, the model does not reproduce well the sub-tidal variability in the east–west direction. The observed along channel mean current at Verrazano Narrows, for the 60-day period from August 1 to September 31, 2002, is shown in Fig. 14, which exhibits a clear two-layered estuarine type of flow with a seaward flow on the surface and a landward flow at the bottom. The mean fresh water

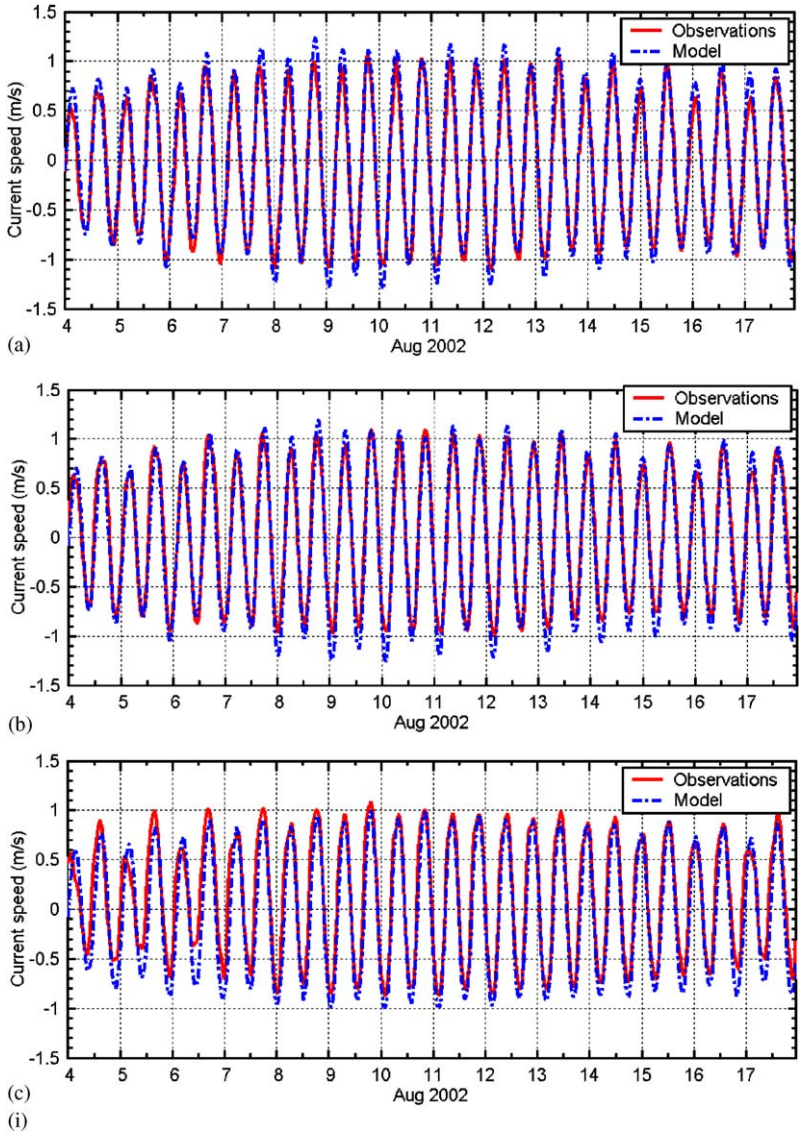

Fig. 12. (i): Comparison of the observed and model-predicted current speeds at (a) surface (22 m from the bottom), (b) mid-depth (15 m from the bottom), and (c) bottom (4 m from the bottom) at Narrows during 4–18, August 2002, (ii): comparison of the observed and model-predicted current speeds (a) at surface (22 m from the bottom), (b) mid-depth (15 m from the bottom), and (c) bottom (2 m from the bottom) at Narrows during 18–30, August 2002, (iii): comparison of the observed and model-predicted current directions at mid-depth at Narrows during 2–30, August 2002.

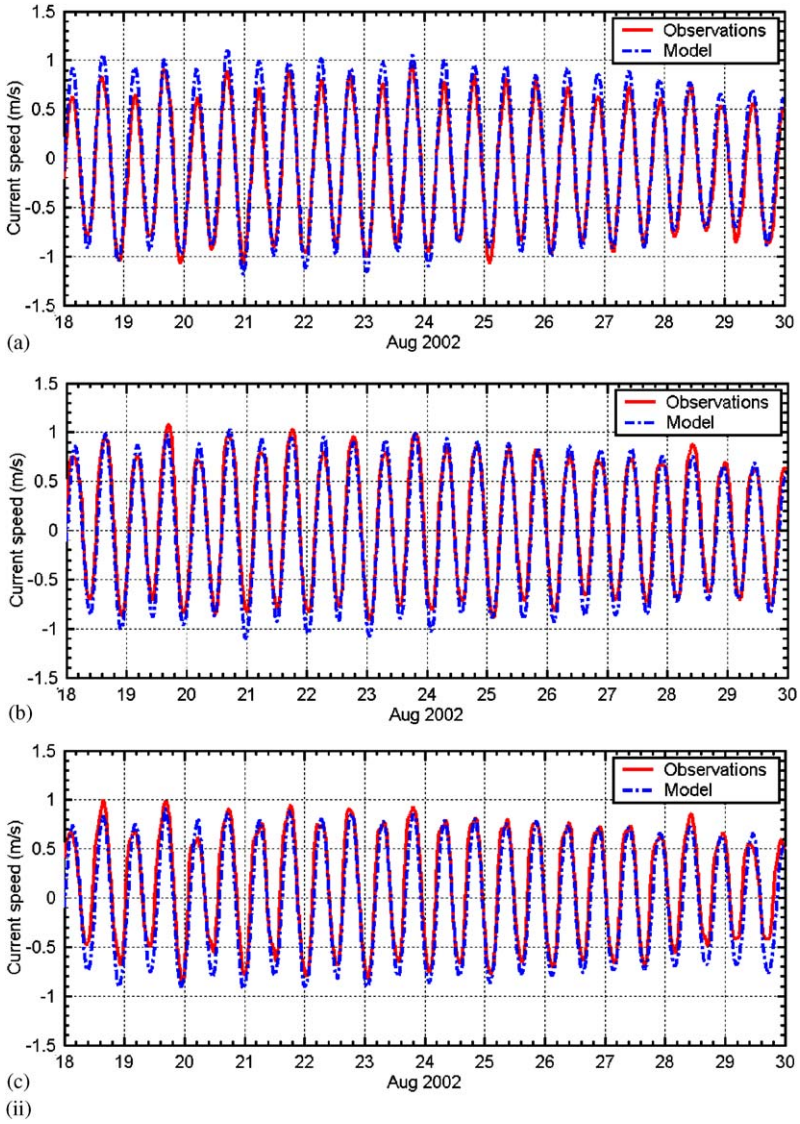

Fig. 12. (*Continued*)

flow from Hudson river during that period was $72\,m^3/s$.

The model-predicted currents and directions at the surface, mid-depth and bottom at Bergen Point compare well with observations as shown in Figs. 15(i) and (ii). The observed and model-predicted current directions at Bergen Point did not show any significant variation in the vertical direction. The model-predicted current directions at mid-depth compare well with the observations shown in Fig. 15(iii). It is seen that the model reproduces the vertical structure of the currents reasonably, with the model slightly over-predicting the ebb currents. A statistical evaluation of the model performance for the three-dimensional currents is given in Table 12. The RMS errors in the model-predicted currents over the depth are within 14% and the correlation coefficients exceed 0.897.

Model-predicted M_2 harmonic principal current speeds and directions at Bergen Point compare well with the observations, as given in Tables 13(a) and (b). The error in the model-predicted M_2 harmonic principal current speed over the depth is within 12% of the observations. The error in the model-predicted principal current directions are within 14.5° of the observations. It is to be noted that ADP

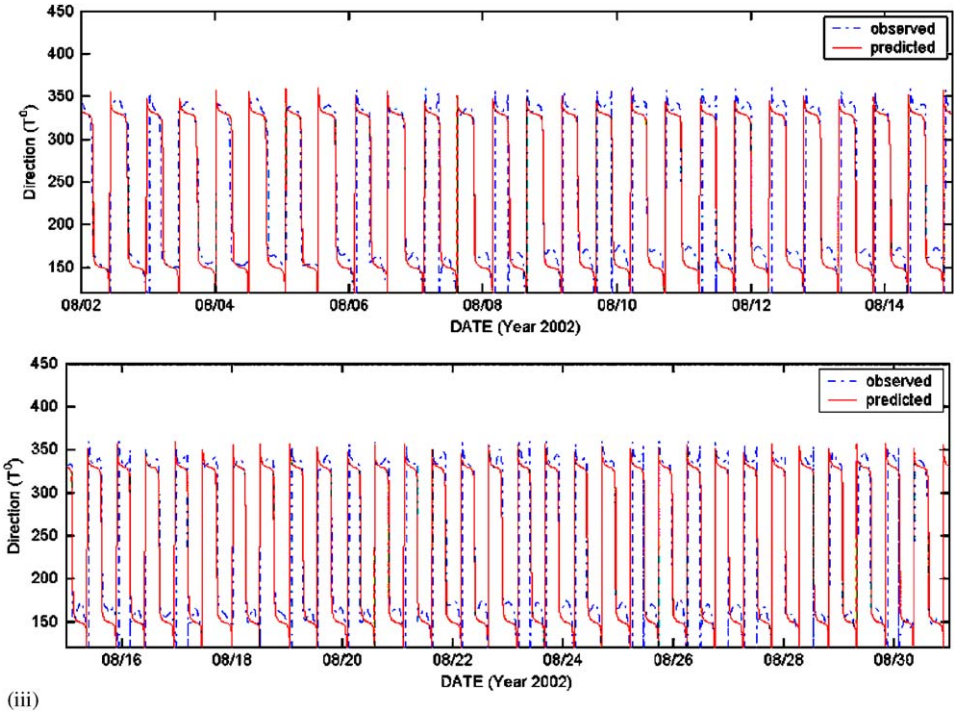

Fig. 12. (*Continued*)

Table 9
Statistical evaluation of model performance for currents at Verrazano Narrows

Depth from bottom (m)	RMS error (m/s)	Data range (m/s)	RMS error (%)	Correlation coefficient
3	0.206	1.863	11.1	0.961
4	0.205	1.951	10.5	0.966
5	0.202	2.024	10.0	0.970
6	0.196	2.077	9.5	0.974
7	0.189	2.113	8.9	0.978
8	0.179	2.141	8.4	0.981
9	0.169	2.158	7.8	0.984
10	0.159	2.163	7.3	0.985
11	0.150	2.159	6.9	0.987
12	0.142	2.145	6.6	0.987
13	0.135	2.105	6.4	0.987
14	0.128	2.095	6.1	0.987
15	0.123	2.087	5.9	0.988
16	0.120	2.093	5.7	0.988
17	0.119	2.123	5.6	0.988
18	0.118	2.144	5.5	0.989
19	0.122	2.178	5.6	0.989
20	0.128	2.210	5.8	0.990
21	0.137	2.243	6.1	0.990

at Bergen Point station is located at the junction of three shallow channels. Hence, a rich spectrum of harmonics and compound constituents is seen from the harmonic analysis of the observed and model-predicted current data at Bergen Point. The model-predicted tidal ellipse parameters for N_2, S_2, and M_4 harmonic constituents show a very good comparison with the observations (Table 14). However, the

Table 10

(a) Comparison of observed and predicted M_2 harmonic principal current speeds and directions

Depth (m) from bottom	Principal current speed (m/s)				Principal current direction current (°T)			
	Observed	95% confidence	Model	Error	Observed	95% confidence	Model	Error
3	0.685	0.012	0.776	−0.091	324.8	1.0	330.7	−5.9
4	0.730	0.011	0.791	−0.061	325.5	0.9	330.7	−5.2
5	0.768	0.013	0.805	−0.037	326.3	0.9	330.7	−4.4
6	0.796	0.013	0.819	−0.023	327.0	0.8	330.7	−3.7
7	0.817	0.012	0.831	−0.014	327.6	0.7	330.6	−3.0
8	0.830	0.013	0.843	−0.013	328.2	0.7	330.6	−2.4
9	0.838	0.012	0.854	−0.016	328.8	0.7	330.6	−1.8
10	0.842	0.014	0.864	−0.022	329.5	0.7	330.6	−1.1
11	0.843	0.013	0.874	−0.031	330.2	0.7	330.6	−0.4
12	0.841	0.014	0.883	−0.042	330.9	0.6	330.6	0.3
13	0.833	0.012	0.890	−0.057	331.7	0.6	330.6	1.1
14	0.828	0.013	0.897	−0.069	333.0	0.6	330.6	2.4
15	0.824	0.012	0.904	−0.080	334.0	0.6	330.6	3.4
16	0.820	0.013	0.909	−0.089	335.1	0.6	330.6	4.5
17	0.818	0.013	0.914	−0.096	336.2	0.6	330.6	5.6
18	0.820	0.011	0.918	−0.098	337.4	0.6	330.6	6.8
19	0.823	0.012	0.921	−0.098	338.3	0.5	330.6	7.7
20	0.828	0.011	0.923	−0.095	339.5	0.6	330.6	8.9
21	0.837	0.010	0.925	−0.088	340.7	0.6	330.6	10.1

(b) Comparison of M_2 harmonic tidal current phases and minor axis currents

Depth (m) from bottom	Phase (°)				Minor axis speed (m/s)		
	Observed	95% conf.	Predicted	Deviation	Observed	95%confidence	Model
3	193.4	1.0	202.9	−9.5	−0.017	0.011	0.026
4	193.8	1.0	203.1	−9.3	−0.011	0.011	0.027
5	194.5	0.9	203.2	−8.7	−0.008	0.012	0.027
6	195.3	0.9	203.3	−8.0	−0.006	0.012	0.027
7	196.3	1.0	203.4	−7.1	−0.005	0.011	0.027
8	197.3	0.8	203.5	−6.2	−0.006	0.011	0.028
9	198.4	0.9	203.6	−5.2	−0.008	0.010	0.028
10	199.3	0.8	203.7	−4.4	−0.010	0.009	0.028
11	200.2	0.8	203.8	−3.6	−0.012	0.010	0.028
12	200.9	0.9	203.9	−3.0	−0.014	0.010	0.028
13	201.7	0.9	204.0	−2.3	−0.013	0.009	0.029
14	202.1	0.8	204.1	−2.0	−0.012	0.008	0.029
15	202.6	0.9	204.1	−1.5	−0.008	0.007	0.029
16	203.0	0.9	204.2	−1.2	−0.003	0.009	0.029
17	203.4	0.9	204.2	−0.8	0.004	0.008	0.029
18	203.6	0.8	204.3	−0.7	0.011	0.008	0.029
19	203.8	0.8	204.3	−0.5	0.023	0.008	0.029
20	203.7	0.8	204.3	−0.6	0.037	0.008	0.029
21	203.6	0.7	204.3	−0.7	0.052	0.008	0.029

model does not reproduce the observed phases well for the M_4 harmonic current with the errors increasing from 20° at the bottom to about 60° near the surface. The model however under-predicts the principal current speeds for M_6 harmonic constituent (Table 14). The model tidal ellipse parameters for the shallow water constituents Mn_4 and Ms_4 are within 95% confidence interval

Table 11

(a) Comparison of observed and predicted tidal harmonic principal current speeds and directions at mid-depth

Depth (m) from bottom	Principal current speed (m/s)				Principal current direction (°T)			
	Observed	95% confidence	Model	Error	Observed	95% confidence	Model	Error
N_2	0.205	0.013	0.179	0.026	328.1	3.1	330.3	−2.2
S_2	0.154	0.013	0.169	−0.015	325.9	3.7	330.3	−4.4
K_1	0.077	0.009	0.069	0.008	330.8	5.0	329.6	1.2
O_1	0.053	0.010	0.044	0.009	336.0	6.6	329.6	6.4
L_2	0.073	0.013	0.038	0.035	335.1	6.9	331.9	3.2

(b) Comparison of observed and predicted tidal harmonic tidal current phases

Depth (m) from bottom	Phase (°)			
	Observed	95% conf.	Model	Error
N_2	191.7	3.6	191.0	0.7
S_2	224.3	4.5	224.6	−0.3
K_1	91.8	7.1	64.6	27.2
O_1	55.7	10.8	24.1	31.6
L_2	200.1	11.9	218.9	−18.8

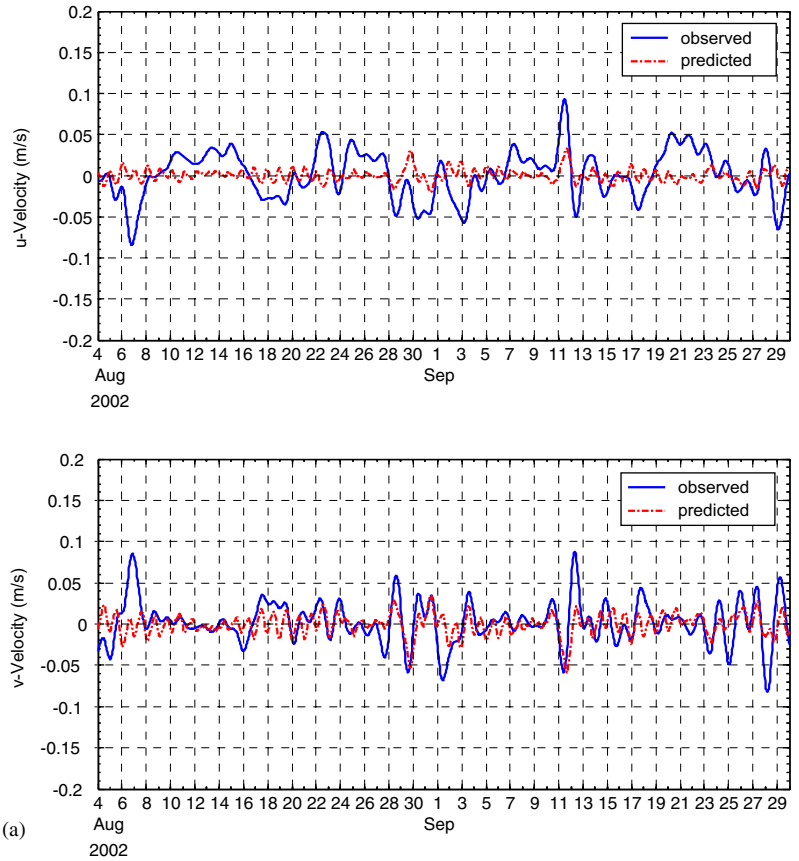

Fig. 13. (a) Comparison of observed and predicted 32-h low-passed near-bottom (4 m from the bottom) currents at Verrazano Narrows, (b) comparison of observed and predicted 32-h low-passed mid-depth (15 m from the bottom) currents at Verrazano Narrows, (c) comparison of observed and predicted 32-h low-passed near-surface (22 m from the bottom) currents at Verrazano Narrows.

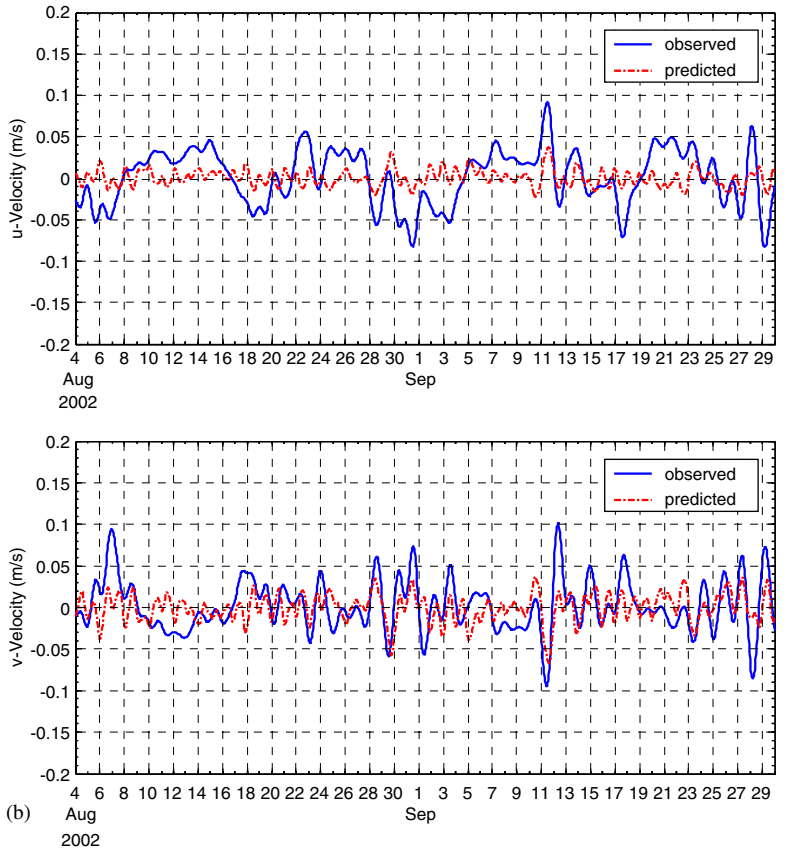

Fig. 13. (*Continued*)

determined from the record (Table 14). It is worth noting that the harmonic constituents M_4, M_6, Mn_4 and Ms_4 together, account for more than 35% of the total tidal energy near Bergen Point. The observed mean currents (Fig. 16) show a net landward flow at Bergen point. The observed and model-predicted sub-tidal currents at Bergen Point were found to be weak (less than 2 cm/s).

The observed M_2 harmonic current amplitudes at College Point and Clason Point in East River (Fig. 3) given in Blumberg and Pritchard (1997) are used to compare the model-predicted M_2 harmonic amplitudes. It is to be noted that both College Point and Clason Point stations are located close to the open boundary in the present study. The model-predicted M_2 harmonic tidal current amplitudes at College Point (Fig. 17a) and Clason Point (Fig. 17b) compare well with observations. The model-predicted M_2 tidal current amplitudes at College Point and Clason Point are within 8 cm/s of the observations.

6. Tidal current distortion in the Harbor region

Along the east coast of US, M_2 is the dominant astronomical constituent and the M_4 tide, a first harmonic of M_2, is the most significant overtide. Transfer of energy to even harmonics can produce asymmetrical tidal velocities. The degree of non-linear tidal distortion in the observed currents at Bergen Point and Narrows can be investigated using the analysis given in Friedrichs and Aubrey (1988). A direct measure of non-linear distortion, the M_4 to M_2 principal current amplitude ratio, can be defined as

$$M_4/M_2 = v_{M_4}/v_{M_2}. \tag{8}$$

The velocity phase of M_4 relative to M_2 can be defined as

$$2M_2 - M_4 = 2\phi_{M_2} - \phi_{M_4}, \tag{9}$$

where v_{M_4} and v_{M_2} are, respectively, the principal harmonic amplitudes of M_2 and M_4 tidal constituents

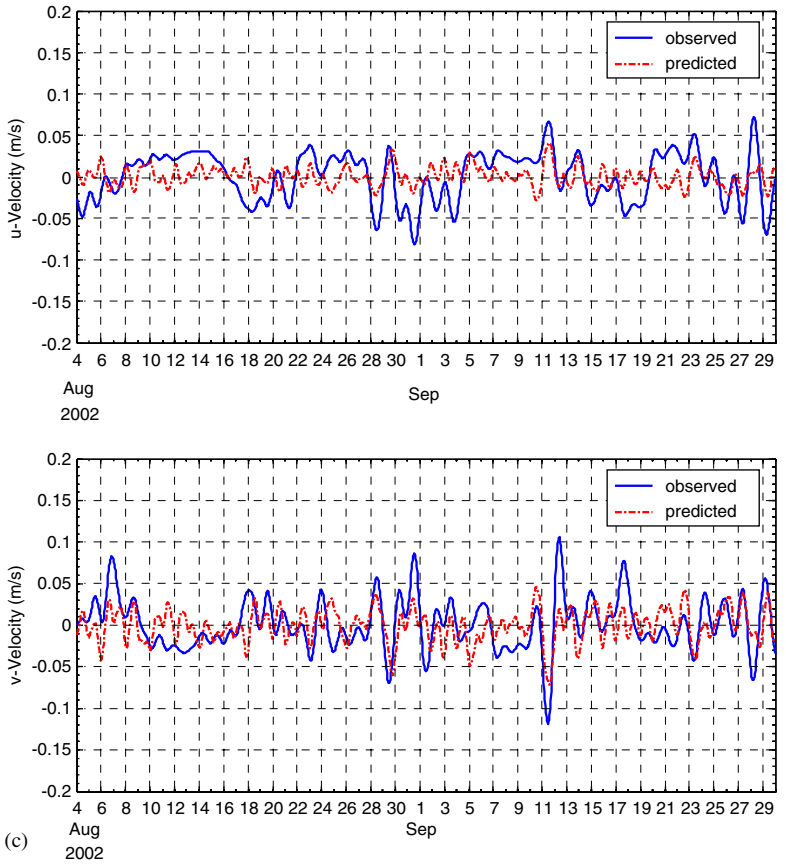

Fig. 13. (*Continued*)

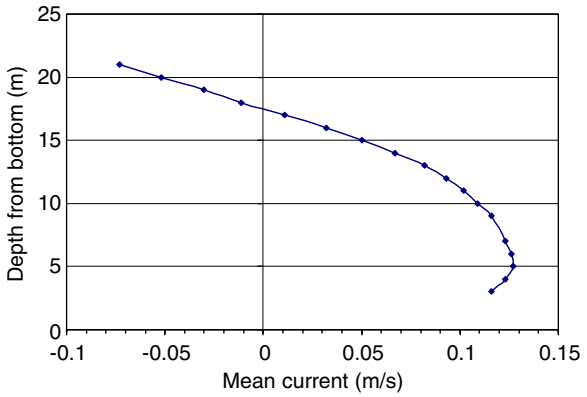

Fig. 14. Observed along channel mean current at Verrazano Narrows.

and ϕ_{M_2} and ϕ_{M_4} are, respectively, the phaselags of the M_2 and M_4 tidal constituents.

If M_4 is locked in a velocity phase of -90° to 90° relative to M_2 with an $M_4/M_2>0$, the distorted composite tide has a higher velocity flood and can be defined as flood dominant. On the other hand, if M_4 is locked in a velocity phase of 90–270° with respect to M_2, the distorted composite tide has higher ebb current and hence can be defined as ebb-dominant. In both cases, the larger the M_4/M_2 ratio, the more distorted the tide and the more strongly flood or ebb-dominant system, it becomes (Friedrichs and Aubrey, 1988).

Table 15 gives the tidal current distortion properties of the currents at Bergen Point and Verrazano Narrows. It is seen that M_4 is locked in a velocity phase of 321.2° (−38.8°) with an M_4/M_2 ratio of 0.19, for the currents at Bergen Point. Thus, the currents at Bergen point can be classified as Flood dominant. This can be confirmed from the time series of currents at Bergen Point, at different depths (Figs. 15(i) and (ii)), which shows that currents are non-linear and asymmetric, with shorter and stronger floods. Time series of model-predicted currents at various locations in Newark Bay, Hackensack and Passaic rivers also showed shorter and stronger floods. Hence, the Newark Bay

system comprising Newark Bay, Hackensack and Passaic Rivers can be classified as a flood-dominant system. The model-predicted currents at Arthur Kill were also found to be flood dominant. These flood-dominant currents (shorter and higher velocity floods) tend to infill their channels with coarse sediments (Boothroyd and Hubbard, 1975; Postma, 1967).

For the currents at Verrazano Narrows, M_4 is locked in a velocity phase of 158.5° with an M_4/M_2 ratio of 0.05. The currents at Verrazano Narrows are nearly symmetric because of their smaller M_4/M_2 current amplitude ratios.

Fig. 18 shows the tidal ellipses for the dominant M_2 harmonic constituent, in the lower New York Harbor region. The model-predicted tidal currents are strongly rotary inside the Raritan Bay, Sandy Hook Bay, and Lower New York Bay, with a clockwise sense of rotation. The model-predicted tidal currents in the Lower Bay, at the entrance to

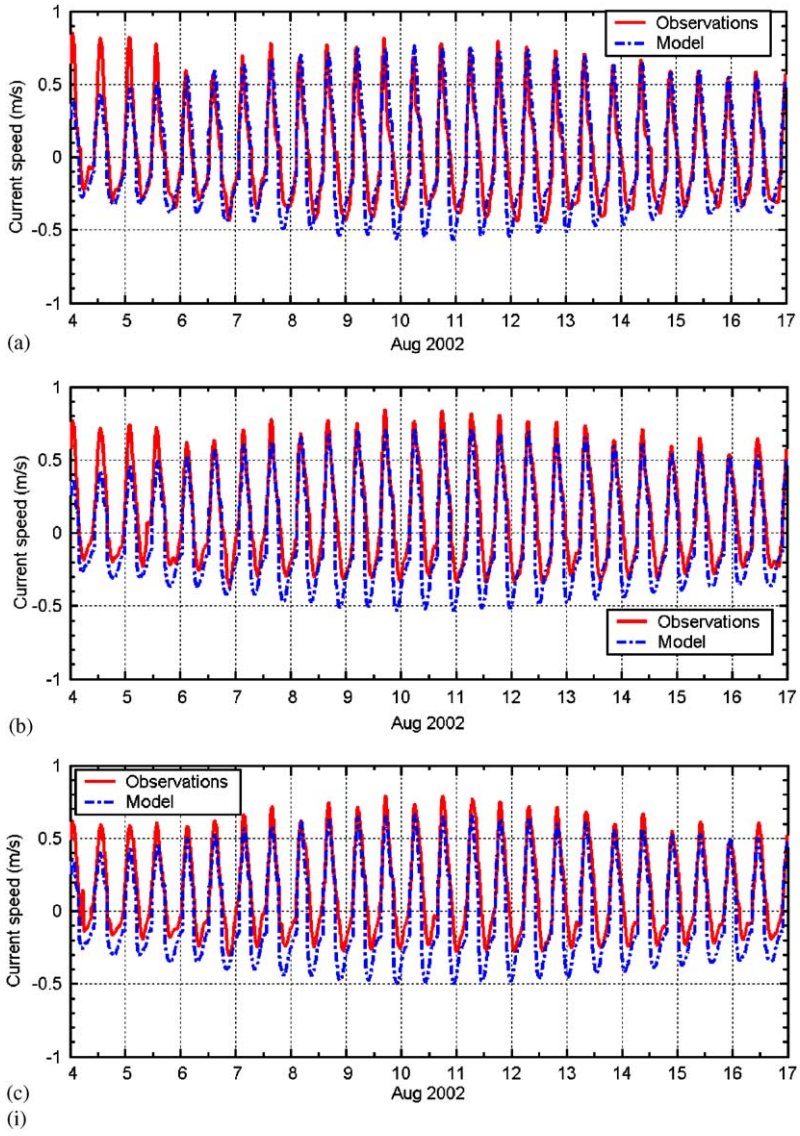

Fig. 15. (i): Comparison of the observed and model-predicted current speeds at (a) surface (9 m from the bottom), (b) mid-depth (5 m from the bottom), and (c) bottom (1 m from the bottom) at Bergen Point during 4–18, August 2002, (ii): comparison of the observed and model-predicted current speeds at (a) surface (9 m from the bottom), (b)mid-depth (5 m from the bottom), and (c) bottom (1 m from the bottom) at Bergen Point during 18–30, August 2002, (iii): comparison of the observed and model-predicted current directions at mid-depth at Bergen Point during August 8–September 15, 2002.

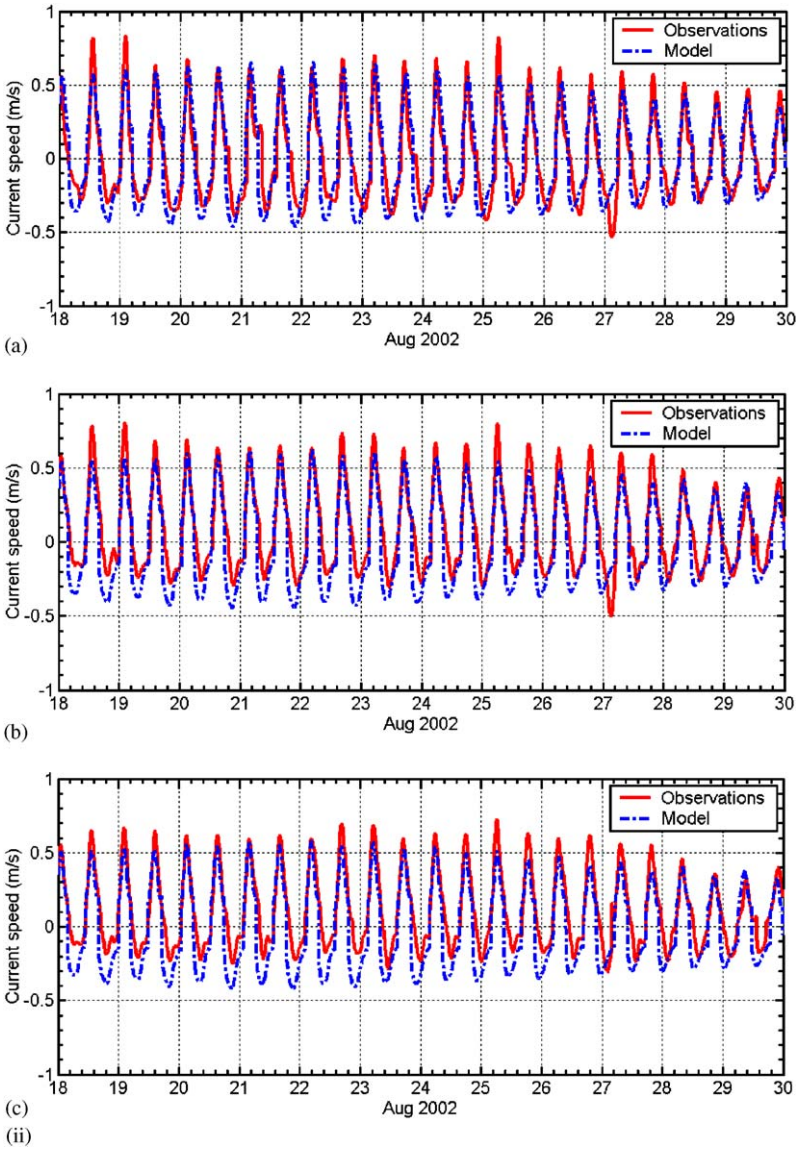

Fig. 15. (*Continued*)

the Jamaica Bay also showed stronger rotary currents, but with an anti-clockwise sense of rotation.

7. Residual currents in New York Harbor

Vertically integrated residual currents were obtained by averaging the model-predicted currents over the 60-day period. It is to be noted that the residual currents computed from this short 60-day simulation does not take into account the seasonal variability of freshwater flows. Fig. 19(a) shows the vertically integrated residual flow field in the Lower, Raritan, and Sandy Hook Bays. The residual flow field shows one counter-clockwise eddy in the Sandy Hook Bay with speeds up to 5 cm/s and another weaker clockwise eddy with speeds up to 3 cm/s in the Lower Bay. The eddy near Sandy Hook is ellipsoidal in shape, with a dimension of 5 km in the east–west direction and 10 km in the north–south direction. The eddy centered around Verrazano Narrows that extends from the Lower Bay to the Upper Bay is corrugated in shape, with a dimension of 6 km in the north–south direction and 600 m in

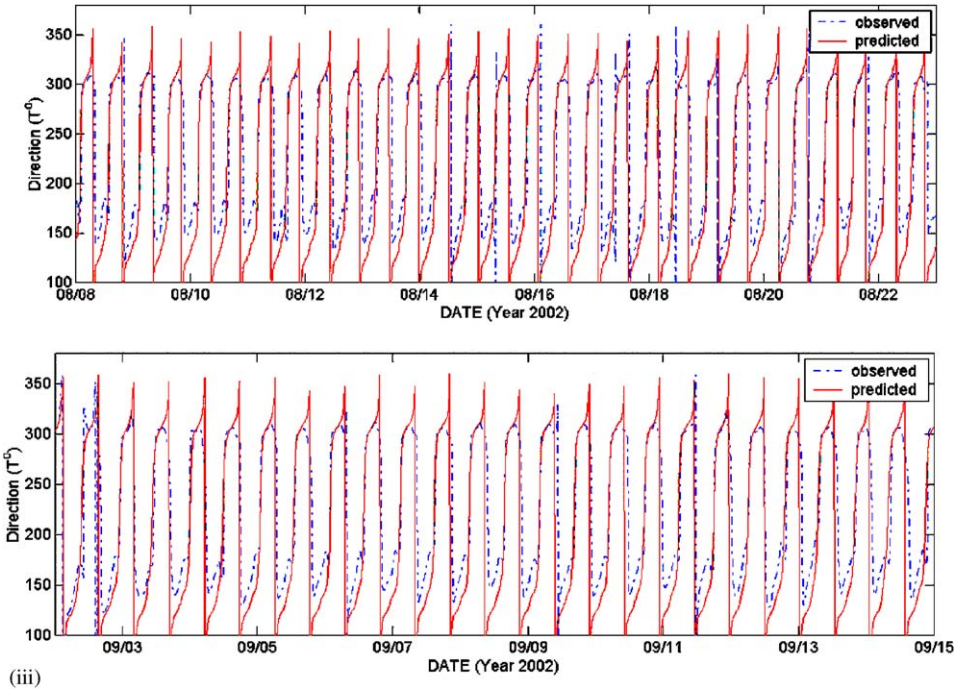

Fig. 15. (*Continued*)

Table 12
Statistical evaluation of model performance for currents at Bergen Point

Depth from bottom (m)	RMS error (m/s)	Data range (m/s)	RMS error (%)	Correlation coefficient
1	0.142	1.044	13.6	0.941
2	0.151	1.099	13.7	0.945
3	0.155	1.300	11.9	0.942
4	0.154	1.303	11.9	0.939
5	0.150	1.345	11.2	0.935
6	0.142	1.221	11.7	0.931
7	0.138	1.235	11.2	0.924
8	0.135	1.259	10.7	0.916
9	0.137	1.427	9.6	0.905
10	0.140	1.382	10.1	0.897
11	0.129	1.315	9.8	0.906

the east–west direction. The occurrence of these eddies is most probably due to the presence of a long headland at Sandy Hook. These residual eddies disappeared when model simulations were run without the advection terms. Though these residual currents were not validated against observations, such residual patterns have been reported in the past. Signell and Geyer (1991) measured and modeled the spatial structure of non-linear tidal flow around a headland in Vineyard Sound, Massachusetts, and showed the occurrence of pronounced flow separation and formation of a pair of counter-rotating eddies at the tip of the headland. The headland at Sandy Hook is much slender and longer than the headland at Gay Head in Vineyard Sound. Fig. 19(b) shows the vertically integrated residual circulation pattern in the Upper and Newark Bays. The model-predicted residual currents showed a counter-clockwise eddy with speeds up to 3 cm/s in the northern end of the Upper Bay and a clockwise eddy with speeds up to 3 cm/s at the mouth of the Newark Bay. Many

Table 13

(a) Comparison of the observed and model-predicted M_2 harmonic principal current speeds and directions

Depth (m) from bottom	Principal current speed (m/s)				Principal current direction (°T)			
	Observed	95% confi.	Predicted	Error	Observed	95% confi.	Model	Error
1	0.322	0.007	0.301	0.021	151.9	1.0	138.6	13.3
2	0.352	0.007	0.315	0.037	152.9	1.1	138.8	14.1
3	0.370	0.008	0.327	0.043	153.5	1.1	139.0	14.5
4	0.379	0.010	0.338	0.041	153.5	1.2	139.2	14.3
5	0.381	0.010	0.347	0.034	153.1	1.2	139.3	13.8
6	0.380	0.011	0.356	0.024	152.4	1.2	139.5	12.9
7	0.376	0.011	0.362	0.014	151.6	1.6	139.6	12.0
8	0.372	0.011	0.368	0.004	150.6	1.7	139.7	10.9
9	0.368	0.009	0.372	−0.004	149.6	1.8	139.8	9.8
10	0.362	0.011	0.375	−0.013	148.5	1.9	139.9	8.6
11	0.339	0.011	0.376	−0.037	144.6	2.6	139.9	4.7

(b) Comparison of observed and model-predicted M_2 harmonic tidal current phases

Depth (m) from bottom	Phase (°)			
	Observed	95% conf.	Model	Deviation
1	299.4	1.3	306.2	−6.8
2	300.8	1.2	306.1	−5.3
3	302.6	1.3	306.1	−3.5
4	304.6	1.3	306.0	−1.4
5	307.0	1.4	306.0	1.0
6	309.4	1.4	305.9	3.5
7	311.8	1.6	305.9	5.9
8	313.9	1.5	305.9	8.0
9	316.1	1.6	305.9	10.2
10	318.3	2.1	305.9	12.4
11	319.6	2.1	305.9	13.7

Table 14

(a) Comparison of observed and predicted tidal harmonic principal current speeds and directions at mid-depth

Depth (m) from bottom	Principal current speed (m/s)				Principal current direction (°T)			
	Observed	95% confidence	Model	Error	Observed	95% confidence	Model	Error
N_2	0.091	0.010	0.083	0.008	309.6	5.5	306.9	2.7
S_2	0.065	0.009	0.068	0.006	316.5	8.6	306.0	10.5
M_4	0.074	0.008	0.068	0.006	298.6	6.6	307.7	−9.1
M_6	0.069	0.010	0.029	0.040	307.0	6.6	306.6	0.4
Mn_4	0.030	0.008	0.031	−0.001	297.0	15.9	307.7	−10.7
Ms_4	0.033	0.007	0.028	0.005	278.7	13.8	308.0	8.2

Table 14 (*Continued*)

(b) Comparison of observed and predicted harmonic tidal current phases and minor axis currents at mid-depth

Depth (m) from bottom	Phase (°)			
	Observed	95% conf.	Model	Error
N_2	150.6	6.0	131.0	19.6
S_2	181.8	6.4	165.0	16.8
M_4	297.6	6.5	343.7	−46.1
M_6	34.0	8.3	52.1	−18.1
Mn_4	297.0	17.2	337.9	−40.9
Ms_4	278.7	15.9	16.7	98.0

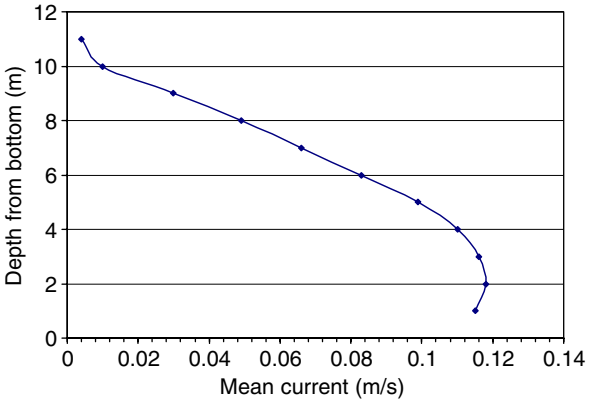

Fig. 16. Observed along channel mean current at Bergen Point.

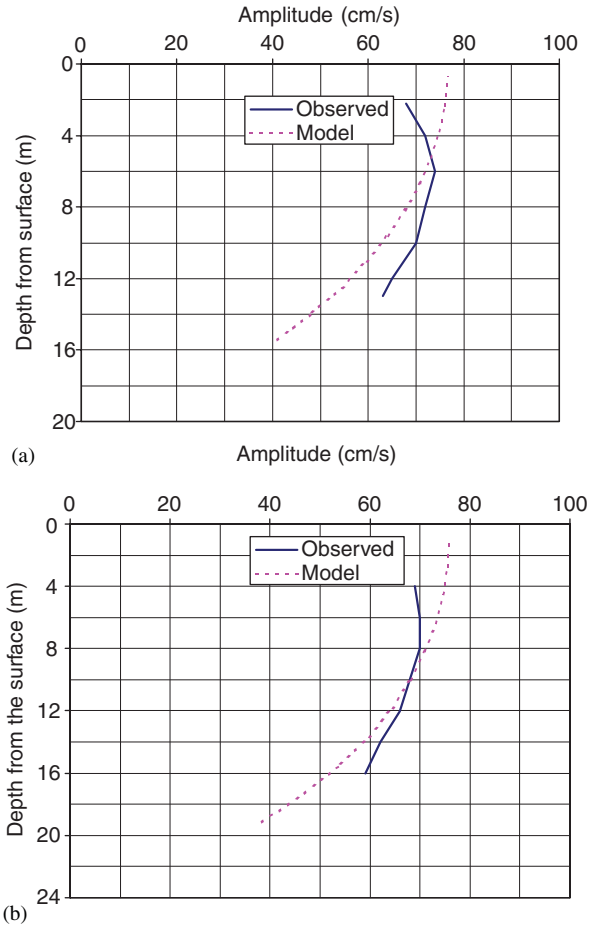

Fig. 17. Comparison of observed (Blumberg and Pritchard, 1997) and predicted M_2 harmonic amplitudes at (a) Clason Point and (b) College Point.

eddies, with speeds as high as 5 cm/s, were seen in Jamaica Bay (Fig. 19(c)), due to the presence of many islands in the Bay.

8. Conclusions

A three-dimensional barotropic hydrodynamic model application to the New York Harbor region was performed using a boundary-fitted coordinate hydrodynamic model developed by Muin and Spaulding (1997a). The model forcing functions consist of surface elevations along the open boundaries, winds on the surface, and fresh water flows from the rivers and sewage outfalls into the study area.

A comprehensive skill assessment of the model predictions is done using observed surface elevations and three-dimensional currents. The model-predicted surface elevations compare well with the observed surface elevations at four stations. Mean errors in the model-predicted surface elevations are less than 4% and correlation coefficients exceed 0.985. Model-predicated three-dimensional currents at Verrazano Narrows show excellent comparison

Table 15
Properties of M_2 and M_4 current harmonics to calculate tidal current distortion

Station	M_2 amplitude (m/s)	M_4 amplitude (m/s)	Ratio of amplitudes M_4/M_2	Phase of M_2 ϕ_{M_2} (°)	Phase of M_4 ϕ_{M_4} (°)	$2\phi_{M_2} - \phi_{M_4}$
Bergen	0.389	0.074	0.19	309.4	297.6	321.2
Narrows	0.841	0.041	0.05	200.9	243.3	158.5

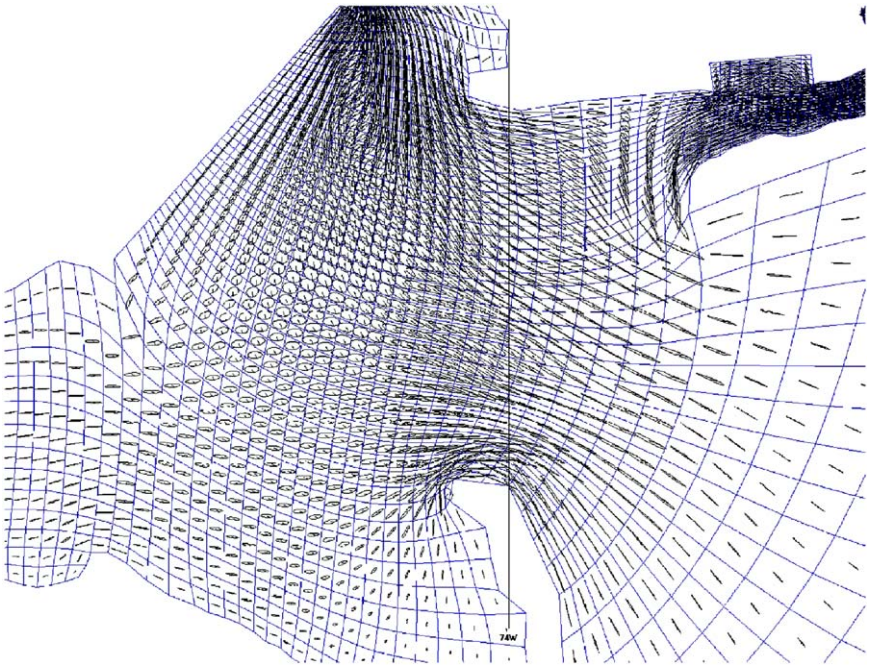

Fig. 18. Tidal ellipses for the M_2 harmonic constituent in the lower bay.

with the observations, with mean errors less than 11% and correlation coefficients exceeding 0.960. Model-predicted three-dimensional currents at Bergen Point compare well with the observations, with mean errors less than 14% and correlation coefficients exceeding 0.897. The model-predicted tidal ellipse parameters at Verrazano Narrows and Bergen Point, for the major tidal constituents, compare well with the observations. The model-predicted tidal ellipse parameters at Bergen Points for the overtides, M_4, M_6, Mn_4, and Ms_4 compare well with the observations. The amplitudes and phases of the principal tidal constituents at nine tidal stations, obtained from a harmonic analysis of a 60-day simulation, compare well with the observed data. The predicted amplitude and phase of the M_2 tidal constituent at these stations are, respectively, within 5 cm and 6° of the observed data. The semi-diurnal tidal ranges and spring and neap tidal cycles of the surface elevations and currents are well reproduced in the model at all stations. The model-predicted sub-tidal elevations and along channel sub-tidal currents compare well with the observations.

Analysis of the observed currents at Bergen Point, using tidal distortion theories, clearly showed the flood dominance in the currents. The model-predicted currents in Newark Bay also showed that Newark Bay is a flood-dominant system, with a potential to infill their channels with coarse sediments. The model-predicted currents at Arthur Kill were also found to be flood dominant.

The model-predicted residual currents in the Lower and Raritan Bays clearly showed two

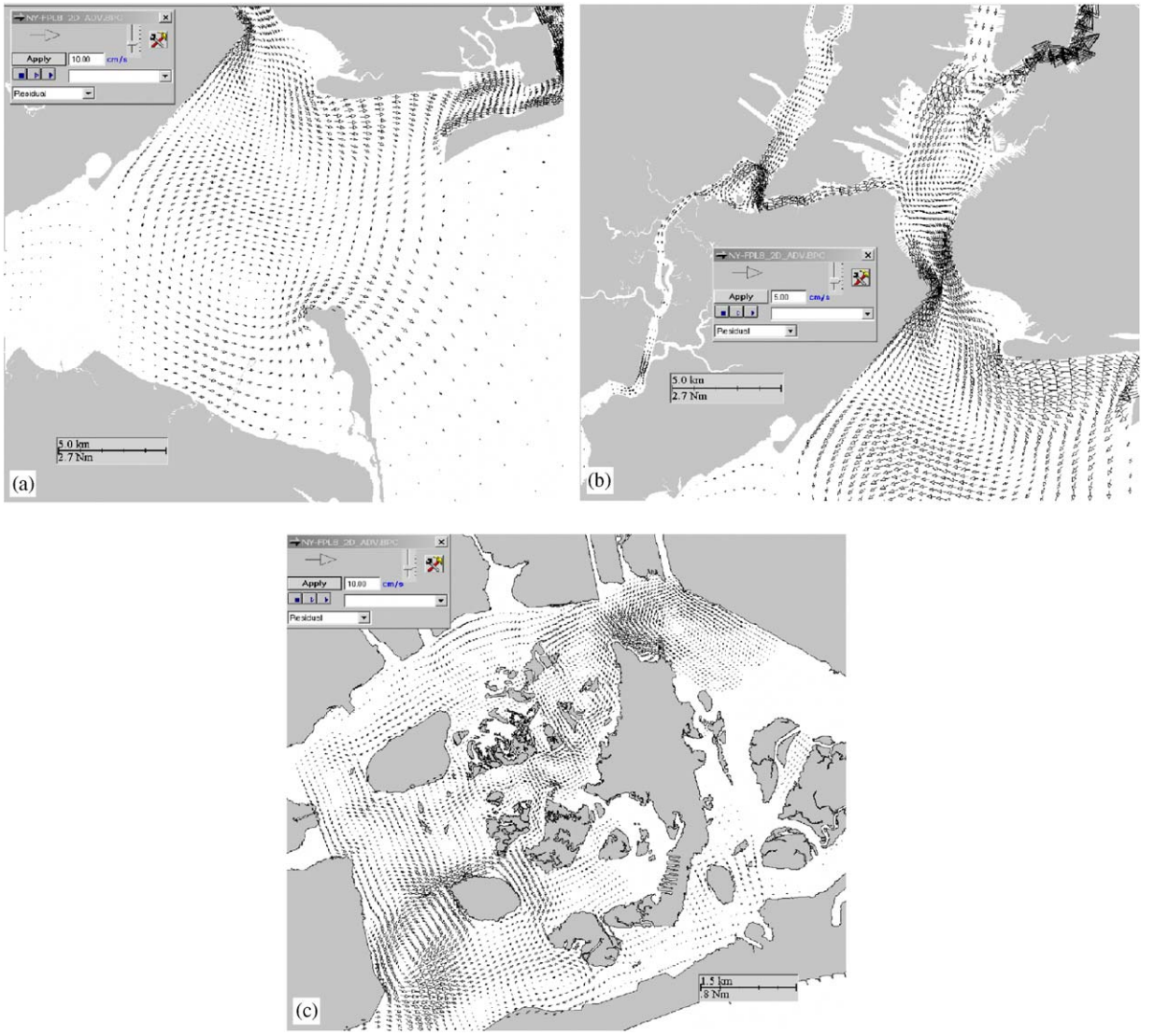

Fig. 19. (a) Vertically integrated residual circulation pattern in the Raritan, Sandy Hook and Upper Bays, (b) residual circulation pattern in the Upper, and Lower Bays, (c) vertically integrated residual circulation pattern in the Jamaica Bay.

counter-rotating eddies, which is attributed to the presence of a headland near Sandy Hook. The model-predicted residual currents showed small-scale eddies in the Upper and Newark Bays. The residual current pattern in Jamaica Bay showed many eddies, with currents as high as 5 cm/s.

Acknowledgments

The author would like to dedicate this paper to his mentor Prof. Malcolm L. Spaulding. Encouragement and support from Dr. Deborah French-McCay during a two-dimensional modeling effort of the study is gratefully appreciated. Many thanks are also due to Ms. Jill J. Rowe for meticulously compiling the coastline and bathymetry for the present study. We would like to thank Mr. Peter Stone of National Ocean Service for providing us with the New York-New Jersey PORTS currents data, and the USGS for providing us the hourly fresh water flow data. Critical reviews of the manuscript from Dr. Gopu Potty and Dr. A.S. Kanmani are very much appreciated. Valuable and insightful comments from the anonymous reviewer and the editor are also very much appreciated.

References

Arakawa, A., Lamb, V.R., 1977. Computational design of the basic dynamical processes of the UCLA General Circulation Model. Methods in Computational Physics 17, 173–265.

Blumberg, A.F., Mellor, G.L., 1987. A description of a three-dimensional coastal ocean circulation model, three-dimensional coastal ocean models. In: Heaps, N. (Ed.), Coastal and Estuarine Sciences, vol. 4. American Geophysical Union, Washington, DC, pp. 1–16.

Blumberg, A.F., Pritchard, D.W., 1997. Estimates of transport through the East River, New York. Journal of Geophysical Research 102 (3), 5685–5703.

Blumberg, A.F., Khan, L.A., John, P.S.J., 1999. Three-dimensional hydrodynamic model of New York Harbor Region. Journal of Hydraulic Engineering 125, 799–816.

Boothroyd, J.C., Hubbard, D.K., 1975. Genesis of bedforms in mesotidal estuaries. In: Cronin, L.E. (Ed.), Estuarine Research, vol. 2, Geology and Engineering. Academic Press, New York, pp. 201–216.

Foreman, M.G.G., 1978. Manual for Tidal Currents and Analysis and Prediction. Pacific Marine Science, Patricia Bay, Sidney, BC, Canada (70pp).

Friedrichs, C.T., Aubrey, D.G., 1988. Non-linear tidal distortion in shallow well-mixed estuaries: a synthesis. Estuarine, Coastal and Shelf Science 27, 521–545.

Moody, J.A., Butman, B., Beardsley, R.C., Brown, W.S., Daifuku, P., Irish, J.D., Mayer, D.A., Mofjeld, H.O., Petrie, B., Ramp, S., Smith, P.C., Wright, W.R., 1984. Atlas of tidal elevation and current observations on the Northeast American continental shelf and slope. United States Geological Survey Bulletin 1611, 122.

Muin, M., Spaulding, M.L., 1996. Two-dimensional boundary-fitted circulation model in spherical coordinates. Journal of Hydraulic Engineering 122 (9), 512–521.

Muin, M., Spaulding, M.L., 1997a. A 3-D boundary-fitted circulation model. Journal of Hydraulic Engineering 123 (1), 2–12.

Muin, M., Spaulding, M.L., 1997b. Application of three dimensional boundary fitted circulation model to Providence River. Journal of Hydraulic Engineering 123 (1), 13–20.

Oey, L.-Y., Mellor, G.L., Hires, R.I., 1985. A three-dimensional simulation of the Hudson-Raritan Estuary. Part I: description of the model and model simulations. Journal of Physical Oceanography 15, 1676–1692.

Postma, H., 1967. Sediment transport and sedimentation in the marine environment. In: Lauff, G.H. (Ed.), Estuaries. American Association for the Advancement of Science Publ. 83, Washington, DC, pp. 158–179.

Sankaranarayanan, S., French McCay, D., 2003a. Three-dimensional modeling of tidal circulation in Bay of Fundy. ASCE Journal of Waterway, Port, Harbor, Coastal and Ocean Engineering 129 (3), 114–123.

Sankaranarayanan, S., French McCay, D., 2003b. Application of a two-dimensional depth-averaged hydrodynamic tidal model. Ocean Engineering 30 (14), 1807–1832.

Sankaranarayanan, S., Spaulding, M.L., 2003. A study of the effects of grid non-orthogonality on the solution of shallow water equations in boundary-fitted coordinate systems. Journal of Computational Physics 184 (1), 299–320.

Signell, R., Geyer, R.W., 1991. Measurements and modeling of the spatial structure of nonlinear tidal flow around a headland. In: Parker, B. (Ed.), Tidal Hydrodynamics. Wiley, New York, p. 883.

Scheffener, N.W., Vemulakonda, S.R., Mark, D.J., Butler, H.L., Kim, K.W., 1994. New York Bight Study, Report I: Hydrodynamic Modeling, Technical Report CERC-94-4, US Army Corps of Engineers, Vicksburg, Mississippi.

Swanson, J.C, Kim, H.S., Sankaranarayanan, S., 2005. Modeling of Temperature Distributions in Mount Hope Bay due to Thermal Discharges from the Brayton Point Station, North-Eastern Naturalist 12(4).